ILLUSORY CONTOUR PROCESSING IN EARLY VISUAL AREAS: A MODELING APPROACH

By

Min Hui

Thesis

Submitted to the Faculty of the

Graduate School of Vanderbilt University

in partial fulfillment of the requirements

for the degree of

MASTER OF ARTS

in

Psychology

December, 2007

Nashville, Tennessee

Approved:

Professor Anna W. Roe

Professor Thomas J. Palmeri

TABLE OF CONTENTS

LIST OF TABLES

Table **Page**

LIST OF FIGURES

CHAPTER I

INTRODUCTION

Introduction to Illusory Contours

The key question in visual neuroscience is how brain mechanisms give rise to visual perception. To address this question, people design stimuli whose physical attributes are characterized in great detail, measure psychophysical and physiological responses of subjects to the stimuli and build computational models to understand the underlying neural algorithms for visual perception in different brain areas. However, the brain goes beyond just mirroring the outside world. Sometimes we perceive things without a direct physical counterpart. This phenomena are often called visual illusions.

This thesis deals with the visual illusions occurred in contour perception, or "illusory contours". Contour perception is critical in human vision in several ways. Firstly, from a computational perspective, contours in 2D domain can provide vital cues about the properties of surfaces in the 3D world, so they are critical in human stereopsis. Secondly, contour provides important cues about the shape of an object and thus it is a key issue for the segregation of objects from the background. Most contours can be defined by luminance contrast. In nature scenes, however, luminance contrast could be very low and defining contour by luminance contrast could be extremely noisy. And sometimes contours could be occluded by other objects, and become discontinuous or incomplete. In these situations, our brain utilize a mechanism of "illusory contour" to deal with these problems and enable us to see object contours which are really not there.

From an evolutionary point of view, the ability to perceive illusory contours is preserved as an adaptive feature of visual system during the process of evolution. Detecting objects in a visual scene can be of vital interest. Potential preys, for example, have to recognize the predator to be

able to escape, or preys can try to hide with the strategy of camouflage, which is to minimize the number of visual cues that distinguish an object from its environment. The predator, on the other hand, strives to break camouflage by exploiting multiple visual cues and interpreting a visual scene. In the case of camouflage, localizing boundaries based on luminance contrast could be low-efficient, and a strategy of combining multiple visual cues (motion, texture, occluding, etc) could lead to a more precise localization (Rivest and Cavanagh 1996). The ability to perceive an illusory contour, therefore, may provide an "anti-camouflage device" (Ramachandran 1987), evolved mainly to detect partly occluded objects.

Illusory contour was first described by Schumann in 1900 as "a percept of borders without physical counterpart in the visual world". Since then a variety of types of illusory contours and their inducers have been discovered and widely used in experiments. These illusory contour stimuli fall into two major categories. One utilizes line ends (e.g., Ehrenstein-figure and abutting line pattern) and the other used incomplete figure (e.g., Kanizsa triangle)(figure 1).

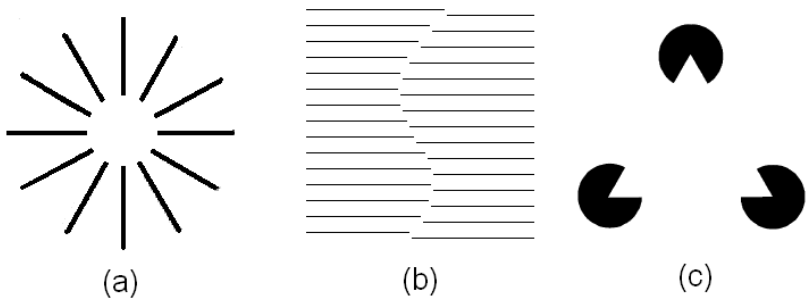

Figure 1. Examples of illusory contour. (a) Ehrenstein figure (b) abutting line pattern (c) Kanizsa triangle

Ehrenstein figure is composed of lines arranged in a circular pattern like rays abutting to the sun. A clear outline of the central circular region is usually perceived. The central part often appears brighter than the outer part, probably because the brightness difference between inner and

outer regions in Ehrenstein figure. Abutting line pattern, presented by Kanizsa 1976, is composed of two sets of lines (parallel or not)with phase displacements abutting to each other. The illusory differs with Ehrenstein figure in that no brightness effect is induced in this illusion. Kanizsa triangle, named after Gaetano Kanizsa, differs with the two illusions introduced above in that it does not use abutting lines as inducers of illusory contour, three partial disks are utilized instead. In this illusion, a non-existing white triangle is usually perceived and it appears brighter than the surrounding area, but in fact it has the same brightness as the background. While these two categories of illusory contour stimuli are widely used in studies of contour processing, a number of other stimulus attributes might also lead to a perception of illusory contour, such as binocular disparity information (Julesz 1960) or dynamic coherence (Cunningham, Shipley and Kellman 1998).

Studies of Illusory Contour Processing

The pioneering physiological studies of illusory contour processing in monkeys were carried out by von der Heydt and Peterhans in 1980s, in which they studied the neural signals in early visual cortex of awake macaques that are tuned to illusory contour stimulation. In their experiment in 1984, they reported that single neurons in V2 responding to illusory contour. V2 neurons responsive to illusory contours were orientation selective and responded stronger to the optimally oriented real line than to the illusory contour of the same orientation. In their following studies Von der Heydt and Peterhans replicated their first findings and showed that V2 neurons can be activated by both Kanizsa-type illusory figures and illusory contours induced by abutting line pattern. They showed that, V2 neurons respond to Kanizsa figures even if the inducers did not touch the receptive field of that cell, which indicated that feedback from higher areas or complex horizontal computations might lead to the cell's response profile.

While V2 cells responding to illusory contour is widely accepted, whether V1 cells respond to illusory contours are more controversial. In Peterhans and Von der Heydt studies,

only very few V1 cells were found to be responsive to illusory contours, while about 32 to 44% of the V2 neurons in their sample were selective for illusory contours. They concluded that V2 is the first area to 'bridge gaps', and that V1 is primarily a contrast edge detector (Peterhans & von der Heydt, 1989). Grosof et al. 1993, however, reported V1 responses to illusory contours of abutting line pattern. This finding of V1 responding to illusory contours has been reproduced by other groups. Lee and Nguyen 2001 recorded single neuron responses in both V1 and V2 to squares in partial disc arrangement, either outlined, modally or amodally completed. What they found was that both V1 and V2 were responsive to real and completed figures, but the earliest responses were found in V2 cells, followed by the V1 responses that emerged at about 100msec after stimulus onset, significantly later than the emergency of V2 responses. Their finding suggests that the neural responses to illusory contour in V1 might be due to feedback from V2.

The involvement of both V1 and V2 in illusory contour was also demonstrated by an optical imaging study (Ramsden, Chou and Roe 2001). In this study, the cortical activity to illusory (induced by abutting line pattern) and real contour stimuli were measured with optical imaging in anaesthetized macaque monkeys. They found that the activation pattern to illusory contour was similar to that of real contour stimuli. In V1, however, the orientation domains of illusory contours were different from real contour orientation domains: domains activated best by vertical real contours were activated best by horizontal illusory contours (figure 2). They proposed that this activation reversal in V1 orientation domains might be due to the feedback from higher areas, possibly V2, and might be a unique "signature" of illusory contour.

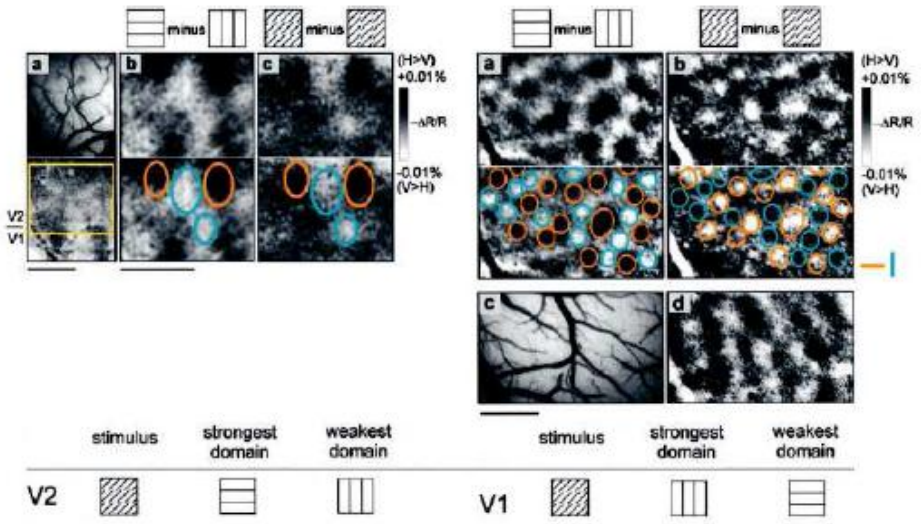

Figure 2 Ramsden et al. 2001. Left, differential optical imaging in V2 shows overlapping orientation maps to illusory and real contour stimulation. Right, real orientation maps in V1 overlap with the activity evoked by the orthogonal illusory contours.

Recent psychophysical study of real-illusory interaction (Dillenburger and Roe 2004) confirms the idea that the feedback from V2 to V1 (Lee and Nguyen 2001) which is orientation reversed (Ramsden, Chou and Roe 2001) might be part of the illusory contour mechanism. In the experiments, illusory contour stimulus was presented for 50 msec after a fixation period of 500 msec. Then real interacting lines were presented for 100 msec after a variable duration of blank screen. The interaction effects were measured by the correction rate of subjects' answer whether the illusory contour were bent out or inwards (Figure 3). In their results, an interaction of real lines and illusory contour dependent on orientation, time and contrast was found. The most consistent effects found in this study are orthogonal low contrast summation effects at an SOA of 50 msec, parallel low contrast interference from SOAs of 125 msec on, and a reversal of orthogonal line effects over all contrast ranges from summation to interference at times of 125 msec to 150 msec.

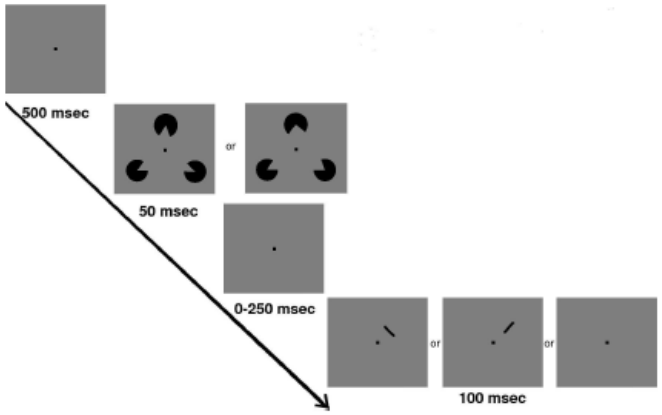

Figure 3. Dillenburger and Roe 2004. A fixation period of 500 msec was followed by the stimulus (50 msec),whose right side was perceived to be either bent out or inwards. After a blank of variable duration (0-250 msec) and real contour presentation (100 msec), subjects had to decide in a 2AFC paradigm, to what side the illusory contour was bent.

Early visual areas (V1 and V2) are ideal for representing the perceived sharp contours explicitly because only the early visual areas contain neurons with small receptive fields that can encode stimulus features with high special resolution. Recent functional imaging experiment, however, found Kanizsa figures elicited significant responses in the lateral occipital (LOC) region, but only weak response in the human early visual areas (Mendola, et al. 1999). Murray et al. 2002 replicated the results by Mendola et al. and measured latencies to illusory figure response onset with EEG and fMRI. They found that the earliest VEP modulation at 88 msec after stimulus onset, which was about 40 msec after the initial visual cortical response. They concluded that illusory contour information in early visual areas might be due to feedback from higher areas such as LOC. Huxlin 2000 reported an observation that the monkey's ability to see illusory contours impaired after a lesion in the inferotemporal cortex (IT) (Huxlin, et al. 2000). Thus, whether illusory contour is an early computation or a late process is still under debate.

In sum, the psychophysical, physiological and functional imaging studies suggested that the processing of illusory contour might take place in multiple brain areas, and complex recurrent intracortical and intercortical connections might be involved.

Proposal of this Thesis

As mentioned in the above section, recent physiological data showed that early visual areas are involved in illusory contour processing. Evidence showed that neural responses to illusory contours in V1 was delayed than V2 (Lee and Nguyen 2001) and the preferred orientation seemed to be reversed to the real contour signal (Ramsden, Chou and Roe 2001). These results suggest a feedback system from primate V2 to V1 might be part of the illusory contour processing mechanism (Roe 2003). Psychophysical studies of real-illusory interactions confirms this idea (Dillenburger and Roe 2004) . An interaction of real and illusory contours depends both on orientation and interaction time was discovered. What they found is that orthogonal real lines tend to enhance the percept first, and interfere later around 125-150 msec, while parallel real lines interfere from 125 msec on, while showing no effect or summation trends at earlier interaction times.

Although physiological and psychophysical data are available to demonstrate that V1 and V2 are involved in illusory contour processing, and that feedback from V2 (Lee & Nguyen 2001) and orientation reversal in V1 (Ramsden et al. 2001) might be part of the illusory contour mechanism, several questions remains to be answered. First, is there a circuitry that can account for the physiological data and psychological data mentioned above? Second, what kind of computation is conducted by early visual cortex that elicits the perception of illusory contours?

Computational modeling provides a powerful tool to address these questions. Computational modeling usually has two approaches. One is a bottom-up modeling approach, which relies heavily on the anatomical and physiological data. Such models can determine whether existing data are sufficient to explain the observed network behavior, and intend to find possible drawbacks and missing components in the model. Another approach is top-down modeling approach, which derives a model from functionality of the neural network. Based on the theoretical analysis, an algorithm that performs the desired function is developed first and then

embedded into the simplified network while imposing known biological constrains (See also Amirikian 1999).

Consider the case of illusory contour processing in early visual cortex, anatomical structures of V1 and V2 have been well studied, but how these structures lead to the network behavior (lagged V1 response to illusory contour stimuli, V1 orientation reversal pattern in illusory contour context, and the orientation dependent illusory contour perceptual strength that varies with) is not clearly known. So in my model, I will make hypothesis about the possible structure of the illusory contour processing circuit based on functionality or network behavior, which is the function-driven part of the model, but some parts of the model will be derived from known anatomical and physiological data, which can be viewed as the data-driven. With computer simulation techniques, the network behavior could be further examined, other properties of the model circuit might be explored. Finally, I will try to propose a possible computational mechanism that will give rise to the illusory contour perception. An outline of the modeling procedure is illustrated in figure 4.

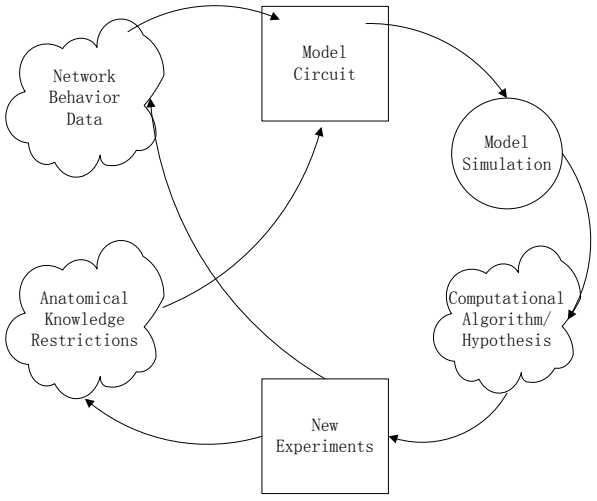

Figure 4. Modeling procedure. See text for detail.

The importance of this computational study is that a model circuit of illusory contour processing in V1 and V2 might point out the direction of future research. New experimental studies might be inspired to test the model. For example, anatomical studies could be conducted to examine the proposed structure of model circuit; physiological experiments could be carried out to test whether the responses of "real circuit" go with the model circuit; and psychophysical studies could be designed to measure the perceptual effects predicted by the computational model.

CHAPTER II

MODEL DISCRIPTION

Model Overview

In this thesis, I suggest that the empirical psychophysical and physiological findings introduced above can be explained within a framework of basic computational mechanisms. A model circuit which includes multiple brain areas with complex intercortical and intracortical connections is proposed here that can explain both the illusory contour inducing process and several accompanying effects found with illusory contour perception introduced before ---i.e., orientation-dependent real-illusory interaction effect that evolves with time (Dillenburger and Roe 2004) and V1 orientation reversal in the abutting line pattern (Ramsden et al. 2001).

A schematic overview of the model is illustrated in Figure 5. The first stage of the model illusory contour processing is the image (illusory contour inducers) feature measurement. In model V1, the local contrast orientation is measured by cells of oriented receptive fields (RFs), such as cortical simple and complex cells and local line ends are measured by hypercomplex end-stopping cells. Thus, V1 serves as a stage of feature measurement and signal detection.

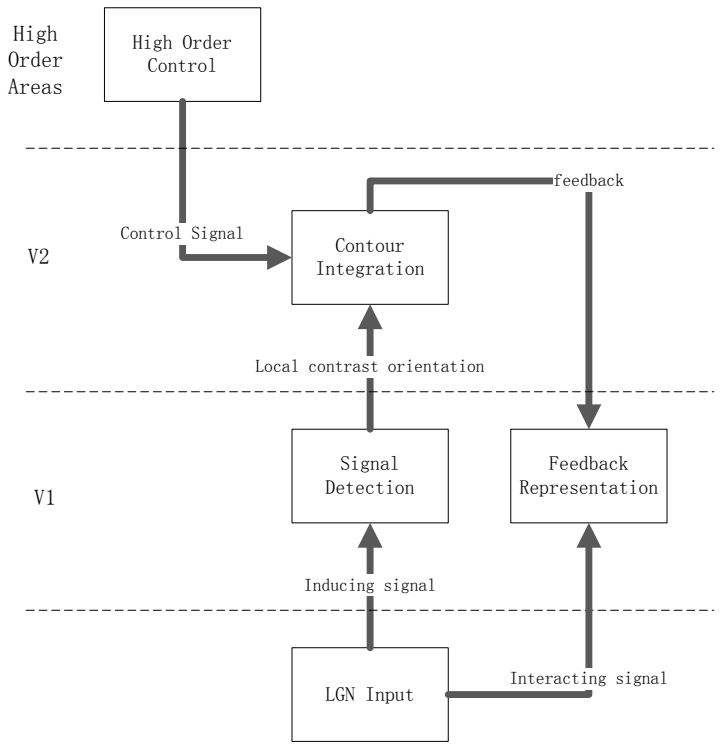

Figure 5. Model overview. Illusory contour perception is a process which contains multiple stages at different brain areas. The first stage of processing is image feature measurement in model V1. Then the resulting activities in V1 are fed into V2 cells with non-classical bipole property which integrate the activities from two distant cells. Contour integration might receive modulation from higher areas. Integrated illusory contour information resides in model V2 was then delivered to model V1 through feedback connection.

The second stage of the model illusory contour processing is contour completion. In my model, V2 is the major brain area where contour completion takes place. After the resulting activities in V1 from local contrast orientations and line ends are fed forward to V2, cells with non-classical bipole property (Grossberg et al. 1997, Neumann and Sepp 1999, Domijan et al. 2007) integrate the activities from two further apart locations and fire at a position that falls in between. Iteration of this process along an oriented path can bridge the gaps between two separate illusory contour inducers. In the model, the non-classical bipole RF property is obtained by lateral connections between V2 oriented cells with similar orientation preferences. In this thesis, a computational model based on activity-dependent synaptic modification was proposed to explain the formation of V2 bipole cell RF property. One thing deserves mentioning here is that whether

horizontal connections in V2 are sufficient for illusory contour induction. Recent fMRI studies in humans (Mendola, et al. 1999, Murray, et al. 2002) suggested that higher areas such as lateral occipital complex (LOC) are involved in illusory contour processing. In order for the neural responses in V2 which arise from lateral connections to be robust, feedback from higher areas such as LOC is likely to modulate the responses in V2.

The third stage of the model involves the feedback projection from V2 illusory oriented cells to V1 orientation domains. This is consistent with the finding that V1 responses are lagged compared to the V2 responses to illusory contours (Lee & Nguyen, 2001). The major concern of this processing stage is how the connection from V2 to V1 mediate a negative feedback in illusory contour context (orientation reversal in V1 orientation domains) and a net excitatory feedback in real line context (Rockland and Douglas 1993, Bullier et al. 1996). My model addressed this complexity with the mechanism of asymmetric positive feedback to V1 and the competition between V1 orthogonal domains. I also showed that the psychophysical data of real-illusory contour interaction (Dillenburger and Roe 2004) could be explained in this framework.

In this chapter, the focus of discussion is on the stage of contour integration in V2 and feedback from V2 to V1 in illusory contour processing. At first, neuron firing rate model was reviewed because it is the basis that the model was built on. The signal detection in V1 has been studied well and discussed by several other authors (Hubel and Wiesel 1968, Mclaughlin, et al. 2000, Neumann and Sepp 1999, Grossberg et al.1997), so it is not discussed in detail in this thesis.

Model Neuron

Neurons are building blocks of circuits, system and the whole brain. And the model proposed in this thesis is also built on the basis of connections between neurons. Therefore, understanding the mechanism of input-output relationship of the neuronal firing rate appears

extremely necessary. Thus, in this section, the computational model of neuronal firing rate is briefly reviewed (See also Dayan and Abbott 2001).

The construction of a firing rate model proceeds in two major steps. First, the relationship between the firing rate of presynaptic neurons and the total synaptic current of a postsynaptic neuron is determined. Second, the firing rate of the postsynaptic neuron should be modeled from its total synaptic current. The relationship between the firing rate and synaptic current is usually measured by injecting current to the neuron. So it is convenient to consider the total synaptic current caused by the membrane conductance change as the current delivered by the presynaptic neurons at each spike arriving.

Consider a neuron receiving N synaptic inputs labeled by $b=1,2,3,\ldots, N$ (Figure 6). The firing rate of the b^{th} input is denoted by u_b. We model how the synaptic current I_s depends on presynaptic firing rates. To do this, we first consider how I_s depends on the presynaptic spikes. If a spike arrives at input neuron b at time zero, we denote the synaptic current generated in the soma of the postsynaptic neuron at time t as $w_b K_s(t)$, where w_b is the synaptic weight and $K_s(t)$ is called the synaptic kernel, which describes the time course of the synaptic current in response to a presynaptic spiking arriving at time t=0. This time course depends on the dynamics of the synaptic conductance activated by the presynaptic spike and also on both the passive and active properties of the dendritic cables that carry the synaptic current to the soma.

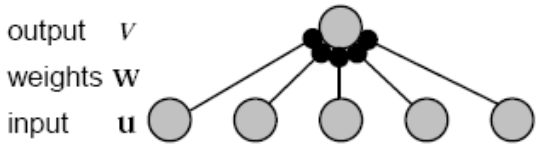

Figure 6. Feedforward inputs to a single neuron. Input rate ***u*** drive a neuron with an output rate *v* through synaptic weights given by the vector ***w***.

The spike train of input neuron b is denoted $\rho_b(\tau) = \sum(\delta(\tau - t_i))$, where t_i is the arriving time of the i^{th} action potential, and $\delta(t)$ is Dirac function. Note that the total synaptic current occurring at input b at times t_i is given by the convolution of the synaptic current that happens after a single spike $w_b K_s(t)$ with the spike train function $\rho_b(t)$.

$$w_b \sum_{t_i<t} K_s(t - t_i) = w_b\, K_s(t) * \rho_b(t) = w_b \int_{-\infty}^{t} K_s(t-\tau)\, \rho_b(\tau) d\tau \qquad (2.2.1)$$

Thus, the total synaptic current coming from all presynaptic inputs can be obtained simply by summing,

$$I_s = \sum_{b=1}^{N} w_b \int_{-\infty}^{t} K_s(t-\tau)\, \rho_b(\tau) d\tau \qquad (2.2.2)$$

Firing rate u(t) is the probability density of firing and is obtained from $\rho_b(t)$ by averaging over trials, so, in a averaging sense, we can replace the spike train function $\rho_b(t)$ in equation 2.2.2 by firing rate of neuron b, namely $u_b(t)$,

$$I_s = \sum_{b=1}^{N} w_b \int_{-\infty}^{t} K_s(t-\tau)\, u_b(\tau) d\tau \qquad (2.2.3)$$

The synaptic kernel most frequently used in firing rate models is an exponential function $K_s(t) = e^{(-t/\tau_r)/\tau_r}$. With this kernel, we can describe I_s by a differential equation if we take the derivative of equation 2.2.3 with respect to *t*,

$$\tau_s \frac{dI_s}{dt} = -I_s + \sum_{b=1}^{N} w_b u_b \qquad (2.2.4)$$

In equation 2.2.4, τ_s is the time constant that describes the decay of the synaptic conductance.

Now consider the relationship between the postsynaptic firing rate and the total synaptic current entering the soma of a postsynaptic neuron. The relationship can be expressed as $v = F(I_s)$, where F is the activation function which is the steady-state firing rate as a function of

somatic input current. F is usually taken to be a saturation function to avoid excessively high firing rates.

The steady-state solution of equation 2.2.4 can be obtained by replacing $\frac{dI_s}{dt}$ with zero, thus we have

$$I_s|_{t=\infty} = \sum_{b=1}^{N} w_b u_b \tag{2.2.5}$$

Plug equation 2.3.5 into the activation function F, and we will have the steady-state firing rate of the post-synaptic neuron with respect to the firing rate of presynaptic neurons,

$$v|_{t=\infty} = F\left(\sum_{b=1}^{N} w_b u_b\right) \tag{2.2.6}$$

Using the activation function F is based on the assumption that the firing-rate changes instantaneously with the total synaptic current. But more often, it is not the case. For this reason, firing rate is often modeled as a low-pass filtered version of the activation function,

$$\tau_r \frac{dv}{dt} = -v + F(I_s) \tag{2.2.7}$$

The constant τ_r in this equation determines how rapidly the firing rate approaches its steady-state value for constant I_s.

If $\tau_r \ll \tau_s$, we can make the approximation that equation 2.2.7 rapidly sets $v = F\big(I_s(t)\big)$. If instead $\tau_s \ll \tau_r$, we can make the approximation that equation 2.2.4 comes to equilibrium quickly compared to equation 2.2.7. Then we can make the replacement $I_s = \sum_{b=1}^{N} w_b u_b$ in equation 2.2.7 and write

$$\tau_r \frac{dv}{dt} = -v + F\left(\sum_{b=1}^{N} w_b u_b\right) \tag{2.2.8}$$

In the computational model circuit proposed in this thesis, we use the firing rate model described by equation 2.2.8.

Lateral Connection: Filling-in the Gap

After the neuronal activities representing the local contrast orientations signaled by V1 neurons are fed forward to higher areas, integration of these separate signals into a representation of a complete contour should take place in a higher area. In my model, I assumed that this proceeds in V2. First, electrophysiological studies showed that V2 cells respond to illusory contours (von der Heydt et al. 1984), and that this response happens prior to the V1 responses to illusory contours (Lee & Nguyen 2001). Second, although several fMRI studies (Mendola, et al. 1999, Murray, et al. 2002) suggested the involvement of high areas in the visual hierarchy in illusory contour processing, the receptive field size of the cells in these areas are too large to make a clear-cut representation of illusory contour. So I suggested that V2 might be a good candidate for the place where contour integrating take place.

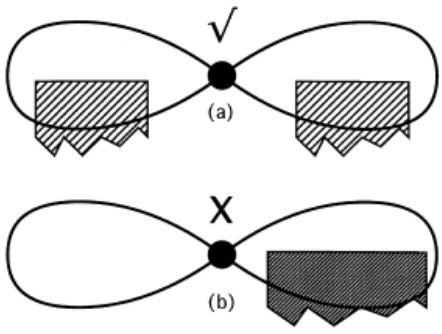

Figure 7. Bipole cell mechanism. A bipole grouping cell can fire: (a) if it receives enough oriented, almost collinear input from both branches of its receptive field; but not (b) if it receives input from only one branch. (See also Ross et al. 2000)

Several computational studies have suggested a "bipole cell" mechanism for spatial grouping and contour integration (Grossberg et al. 1997, Neumann and Sepp 1999, Ross et al. 2000, Domijan et al. 2007). A bipole cell is supposed to have a receptive field with two spatially separate lobes, and it performs an AND-gate function of the activities from these two separate lobes. Such a cell will be activated only when it receives input from both of the lobes (Figure 7).

The bipole cell hypothesis found strong support from anatomical studies of long range lateral connection in tree shrew cortex (Bosking et al. 1997). Cells with long range connections in cortex were found to contact cells of similar orientational preference and the receptive field centers of the contact cells are aligned in the cortical map along directions that correspond to the orientational preference of the cell forming the axonal connection (Figure 8).

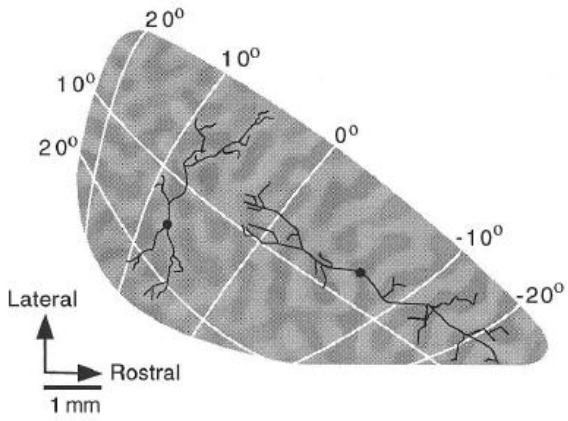

Figure 8. Specificity of horizontal connections between V1 cells of layer 2/3. Axon arborizations from two example cells are shown over a combined map of visual space and orientation preference (dark regions cells with 90 deg orientation preference; light regions cells with 0 deg preference). The cell in a dark region of the map projects to other areas with the same orientation preference (90 deg). Moreover, those cells that were selectively contacted lie along a line that is orthogonal to the 0 deg meridian. The other cell in a light region of the map projects to spatially distant cells with the same orientation preference (0 deg) that lie along a line parallel to the 0 deg meridian. (From Bosking *et al*. 1997)

In computational modeling of a bipole cell, we are especially interested in (1) the dendritic structure of a bipole cell, that is, how the cell interact with other cells with similar orientation preference through lateral connection and how the weights of these connections distribute spatially, and (2) the mechanism of the bipole property, that is, how the cell perform the AND-gate function. Clearly understanding these points, contour integration can be performed simply by spatial-filtering the input pattern (V2 activation fed from V1) with templates which ensembles the spatial weighting function of a bipole cell. In this section, great emphasize is on developing a computational model for the spatial distribution of synaptic weights of horizontal connections, while the mechanism of bipole property proposed by other studies are briefly reviewed.

Existing models of a bipole cell determine the spatial weighting function mainly from the geometric relationship, with little emphasize on the underlying biological basis of the formation

of such a bipole structure, thus, the spatial weighting function is often preprogrammed. In this section, the spatial weighting function of a bipole icon is obtained by modeling the synaptic plasticity of long-range horizontal connections that link the neurons with similar orientation preferences. Other than a preprogrammed spatial weighting, such a model is self-assembled which requires a minimum number of pre-defined parameters.

There are several basic assumptions about this model. First, the modular orientation specificity and axis orientation specificity of the long-range horizontal connections could be explained in a developmental framework. I assume that, in immature brain, no such specificities should exist and these properties of long-range horizontal connections are formed through visual experience. Second, straight lines should be the major type of visual experience which can give rise to the modular orientation specificity and axis orientation specificity of long-range horizontal connections. In nature scenes, we experience straight line or its approximation more frequently than a curve with large curvature. The latter exists mainly in visual scenes with high spatial frequency or in a relatively small scale, which does not match the scale of a long-range horizontal connection.

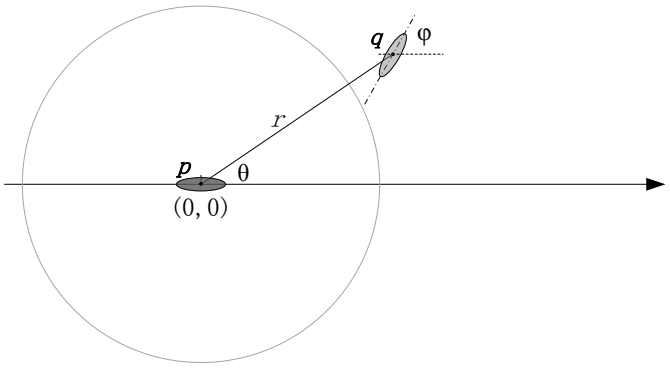

Figure 9. Spatial relationship of bipole cell and a distant input cell. A bipole cell *p* with horizontal orientation preference is positioned at the origin of the coordinate (dark ellipse). Another oriented cell *q* (light ellipse), locates at the position of $(\boldsymbol{r}, \boldsymbol{\theta})$, and has an orientation preference of $\boldsymbol{\varphi}$. The model asks for the synaptic weight $\boldsymbol{w}(\boldsymbol{r}, \boldsymbol{\theta}, \boldsymbol{\varphi})$ between these two cells.

Consider the polar coordinate in Figure 9. A bipole cell p is positioned at the origin of the coordinate $(0,0)$, marked by a dark ellipse, has an orientation preference of 0 degree. Another oriented cell q, marked by a light ellipse, locates at the position of (r, θ), and has an orientation preference of φ. The quantity to be assessed here is the contribution of activation of cell q to the activation of cell p, or the synaptic weight of the connection from q to p. The synaptic weight $w(r, \theta, \varphi)$ is the spatial weighting function, which changes with the combination of (r, θ, φ). First, $w(r, \theta, \varphi)$ is distance dependent because horizontal connection has a limited extent which typically is about 20 degrees of the visual world. Second, $w(r, \theta, \varphi)$ depends on the orientation preference φ of the input cell q and its angle position θ, because too large deviation of these angles from zero would result in a weak relatability of cell p and q.

For simplicity, I assume that the spatial weighting function $w(r, \theta, \varphi)$ is parameter-separatable,

$$w(r, \theta, \varphi) = w(r)w(\theta, \varphi) \tag{2.3.1}$$

Thus, we can consider how each of the independent variables contribute to the spatial weighting function separately.

Spatial weighting dependence on angles

How this kind of spatial pattern of synaptic weight distributes as a function of axis angle θ and φ? As I already assumed, this kind of distribution is accomplished by the activity dependent synaptic strength modification. The general law of this kind of modification is Hebb's rule, which implies that simultaneous pre- and postsynaptic firing increases synaptic strength, whereas uncorrelated firing eliminate synapses. This activity-dependent progress could be described using the following differential equation,

$$\tau_w \frac{dw}{dt} = (v - \varepsilon)u \tag{2.3.2}$$

In equation 2.3.2, w is synaptic weight that evolves with time, u and v are pre-and post synaptic firing rate respectively. τ_w is the time constant of the synaptic weight change. The complication in this equation lies in ε, a factor used to constrain the unlimited growth of synaptic weight growth. The idea underlying equation 2.3.2 is that, when the presynaptic firing rate u is accompanied by a large enough postsynaptic firing rate v, the strength of the synapse will increase, otherwise it will decrease.

Back to the spatial weighting function problem, the inputs to a bipole cell p are the intercortical feedforward input from V1 and the intracortical inputs from V2 oriented cells through horizontal connections. In immature brain, the horizontal connections are assumed to exhibit no axis specificity. Thus, at time $t = 0$, the horizontal connections from input cells in V2 positioned at all directions and with all possible orientation preferences contribute equally to the postsynaptic neuron p.(Figure 10)

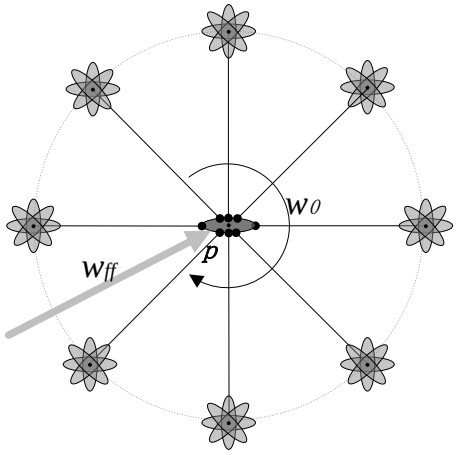

Figure 10 Horizontal connection pattern at initial time. At time $\boldsymbol{t = 0}$, the horizontal connections from input cells in V2 positioned at all directions and with all possible orientation preferences contribute equally to the postsynaptic neuron p, with the initial synaptic weight w_0. Bipole cell p also receives feedforward input (grey arrow) from V1 with a synaptic weight w_{ff}.

For simplicity, I divided the infinite number of possible directions θ and φ into a finite number N of angles. Thus an integer pair (n,m) can be used to represent the pair of (θ,φ),

$$(\theta, \varphi) = \left(\frac{2\pi}{N} n, \frac{2\pi}{N} m\right) \tag{2.3.3}$$

The problem now evolves into one that asks how $w(n, m)$ change with time due to the correlation of activities of pre and post synaptic neurons. Remember another assumption we have made previously is that straight lines should be the visual stimuli that give rise to the spatial pattern of weighting function in the model. Given a straight line stimulus with a spatial orientation *n*, suppose it goes across bipole cell *p*, cell *p* will receive synaptic input from (1) the feedforward input from V1 orientation cell, (2) the activation sent from cells with angle position *n* and with variable preferred orientation of *m*. Therefore, firing rate of cell *p* with a straight line of orientation *n* can be written as,

$$v(n, m) = w_{ff} f\left(n \frac{2\pi}{N}\right) + w(n, m) u(n, m) \tag{2.3.4}$$

In Equation 2.3.4, w_{ff} is the synaptic weight of feedforward connection from V1 to cell *p*; *f* is the orientation tuning function of the V1 cell with preferred orientation of zero degree; *w(n)* is the synaptic weight of a neuron at the angle position of *n* and with a orientation preference of *m*, and *u(n,m)* is the firing rate of this neuron, which can also be written using V1 orientation tuning function *f*.

$$u(n, m) = w_{ff} f\left((n - m) \frac{2\pi}{N}\right) \tag{2.3.5}$$

Rewrite Equation 2.3.2 with respect to the spatial orientation of *n*, we have,

$$\tau_w \frac{dw(n, m)}{dt} = (v(n, m) - \varepsilon) u(n, m) \tag{2.3.6}$$

To avoid unstable growth of *w*(*n*,*m*), we use a sliding threshold ε in Equation 2.3.6,

$$\varepsilon = \frac{\sum_{w>0} v(n, m)}{N|_{w>0}} \tag{2.3.7}$$

Note that ε has a complex relationship with the postsynaptic firing rate of cell *p*. This relationship can be described as the average firing rate of cell *p* across all axis directions and

orientation preferences such that the synaptic weights of horizontal connections of those direction are non-zero. Substitute Equation 2.3.7 into 2.3.6 and sum under the condition of $w(n,m)>0$,

$$\sum_{w>0} \tau_w \frac{dw(n,m)}{dt} = \sum_{w>0} (v(n,m) - \varepsilon)u(n,m)$$

$$\tau_w \frac{d\sum_{w>0} w(n,m)}{dt} = \left(\sum_{w>0} v(n,m) - \sum_{w>0} \varepsilon\right)u(n,m)$$

$$= \left(\sum_{w>0} v(n,m) - \sum_{w>0} \left(\frac{\sum_{w>0} v(n,m)}{N|_{w>0}}\right)\right)u(n,m)$$

$$= \left(\sum_{w>0} v(n,m) - N|_{w>0} \frac{\sum_{w>0} v(n,m)}{N|_{w>0}}\right)u(n,m)$$

$$= 0 \qquad (2.3.8)$$

Equation 2.3.8 implies that the total synaptic weight on cell p is time- invariant. This controls the unlimited growth of synaptic weights and is consistent with the concept of synaptic capacity, which implies that the total number of synapse on a neuron is a constant number, and the modification of synaptic weight is a process of re-allocation of synapses among input neurons.

Obtaining the analytical solution to Equation 2.3.6 could be extremely complicated because the sliding threshold ε has a nonlinear and implicit relationship with the dependent variable w. The approach to solve a differential equation like that is to convert the differential equation to a difference equation which can be solved numerically, as will be discussed in detail in the next chapter. Here we can make a conceptual analysis of the form of solution of 2.3.6. For simplicity, we only consider the situation when V1 distant input cells (q) were optimally oriented ($\theta=\varphi$, or $n=m$). The initial state of $w(n)$ is $w(n)|_{t=0}=w_{0,}$ which implies a homogeneous distribution of synaptic weights across all N orientations. Then at those directions such that $v(n)$ is above average, synaptic strength will be increased and those below average will be decreased, which causes an spatial inhomogeneity across the N directions. This inhomogeniety increases with time until at a point some synaptic weights are decreased to zero and thus synapses are eliminated.

The remaining directions will go through a similar process as described above, and ultimately the synaptic weights will be distributed around a line parallel to the preferred orientation of bipole cell.

Spatial weighting dependence on distance

As assumed earlier, spatial weighting function $w(r,\theta,\varphi)$ is parameter-separatable, $w(r,\theta,\varphi) = w(r)w(\theta,\varphi)$. In last section, we proposed a computational model based on activity dependent synaptic modification to address the spatial weighting dependence on angle combination(θ,φ). A system of differential equations were developed to describe the model. And a conceptual analysis was made to demonstrate the form of synaptic weight distribution across axis angles. Now we address the question how synaptic weighting distribute as a function of distance r.

In our model, the synaptic weighting dependent on distance, $w(r)$, was modeled as a Gaussian function

$$w(r) = \frac{1}{r_0\sqrt{2\pi}} e^{-r^2/2{r_0}^2} \tag{2.3.9}$$

Synaptic weight decreases with increasing distance. How could this be interpreted? I think this could also be explained within a framework of activity-dependent synaptic modification. Action potentials conduct along neuron axons at the finite velocity, and evidence showed that signal conduction is significantly slower in lateral connections than feedforward and feedback connections. With large distance r, the correlation of firing pattern will decrease, and so will the synaptic weights at large distance. Why is it reasonable to model distance r and angle (θ,φ) as parameter separatable? My explanation is that the synaptic weight dependence on distance underlie a universal process of synaptic modification, which is independent of the type of stimulus and visual experience. So at each axis angle and orientation preference, a similar

process of synaptic modification dependent on distance takes place. Therefore, distance r and angle (θ, φ) are parameter-separatable in the model.

In summary, I proposed a model based on activity-dependent synaptic modification to explain the mechanism of lateral connection formation in this section. With the assumption that straight lines are the major visual experience leading to the specific configuration of bipole cell receptive field, a system of non-linear differential equations that depends on internal states of equation solution was built to describe the model. The concentration of discussion in this section was on the relationship between synaptic weight of lateral connection in V2 and spatial attributes (spatial location and orientation preferences). Models of AND-gate function of a bipole cell have been proposed by several authors. Grossberg, Mingolla and Ross 1997 attributed the bipole property to the activation of smooth stellate cells. In their model, the distant input cells target not only the bipole cell, but a common inhibitory stellate cell near the bipole cell as well. The stellate cell is proposed to inhibit the activation of bipole cell when only one branch of the bipole receptive field gets stimulated and easily become saturated and fails to neutralize the excitatory inputs to the bipole cell when both branches are stimulated, thus leading to the bipole property. Other than Grossberg's approach, Neumann 1999 explained the formation of bipole property with a model circuit of three processing stages. The signals from both branches of the bipole receptive field are integrated in such a circuit and finally form an output signal which is the logic-AND of the signals from two branches. A recent model based on dendritic computation was proposed to explain bipole property in illusory contour formation (Domijan et al. 2007). In their model, the bipole cell sum inputs along its dendritic branches. Outputs from dendritic branches multiplicatively interact before they reach the soma, and this kind of dendritic computation was shown to give rise to the logical AND function.

Feedback from V2 to V1

The earliest neuronal response to illusory contour stimulation has been found in area V2 (Peterhans and von der Heydt 1989, von der Heydt and Peterhans 1989, Lee and Nguyen 2001). An activation of V1 which was delayed relative to the V2 signal was reported by Lee & Nguyen 2001, confirming previous reports of illusory contour related activity in the first visual cortical area (Grosof et al. 1993, Sheth et al. 1996, Ramsden, Chou and Roe 2001). The temporal delay of the V1 activation relative to V2 might suggest that feedback from V2 might lead to illusory contour responses in V1 (Lee and Nguyen 2001). Illusory contour activity in V1 furthermore has been shown to be reverse oriented to real contour activity (Sheth et al. 1996, Ramsden, Chou and Roe 2001)

Psychophysical studies of real-illusory interactions confirms the feedback system from V2 to V1 involved in contour processing (Dillenburger and Roe 2004). An interaction of real and illusory contours depends both on orientation and interaction time was discovered. Orthogonal real lines tend to enhance the percept first, and interfere later around 125-150 msec, which is consistent with the transition from V2 activation to V1 activation (Lee and Nguyen 2001) . Parallel real lines interfere in general from 125 msec on, while showing no effect or summation trends at earlier interaction times.

How is the feedback connection from V2 to V1 configured so that it can give rise to the physiological and psychophysical evidences stated above? Although the feedback from V2 to V1 has been studied (Bullier et al. 1996, Girard et al. 2001, Shmuel et al. 2005), the answer to this question is still unclear. A computational model of the feedback circuit from V2 to V1 which fit the physiological and psychological data as well as known anatomical knowledge will greatly facilitate our understanding of illusory contour processing and possibly inspire future experimental studies. So in this section, I will try to build a model circuit that fits the data available.

A schematic view of the model feedback circuitry is illustrated in Figure 11. Four neurons u_1 through u_4 consist of the model system, in which u_1 and u_3 are V1 oriented neurons with orientation preference of 0 deg and 90 deg respectively, while u_2 and u_4 are V2 neurons responsive to both real and illusory oriented lines with orientation preferences of 0 deg and 90 deg respectively. Connections between the neurons are illustrated by the dot-head lines with a corresponding synaptic weight, and black dots represent synapses. For simplicity, I assume that the connection configuration are the same across different orientation columns, on Figure 11 this is illustrated by the symmetric connection configuration pattern between the 0 deg part (upper) and 90 deg part (lower). An explanation of all connections between the neurons are listed in Table 1.

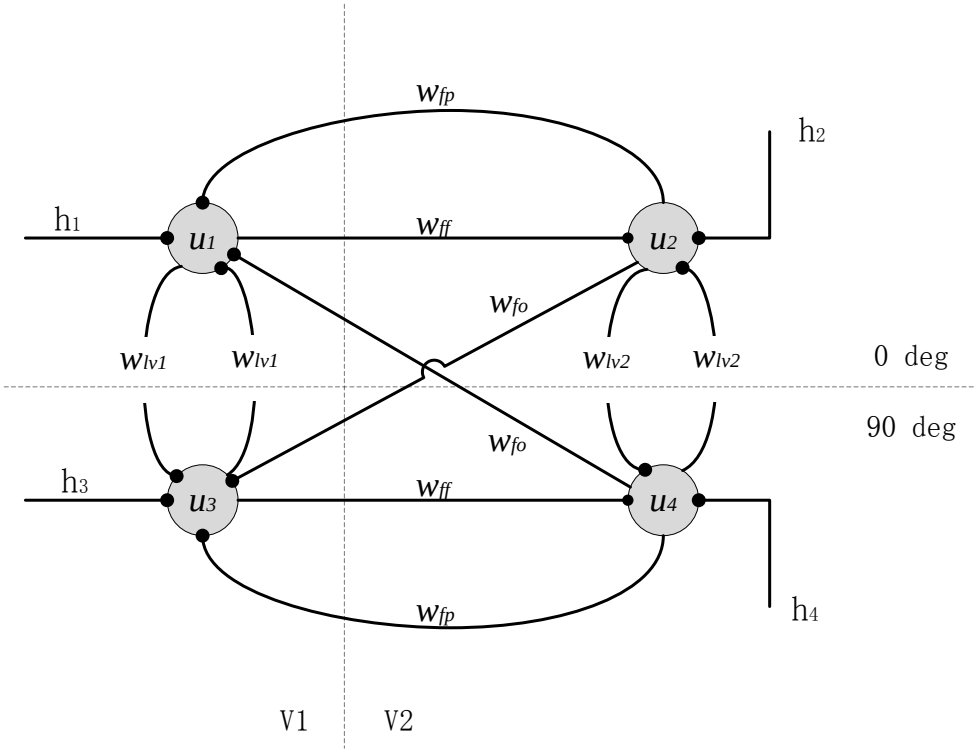

Figure 11. Model feedback circuit involved in illusory contour processing. Four neurons u1…u4 are V1 horizontal cell, V2 horizontal cell, V1 vertical cell and V2 vertical cell respectively.h_1 through h_4 are the inputs to the circuit, measured by presynaptic cell activation. While h_1 and h_3 are feedforward input from LGN to V1 orientation domains, h_2 and h_4 contain mainly the activation from horizontal connections in V2.

Table 1. Connection description in Figure 11

Type of Conn.	Connections	Description
System Input	(, h_1, u_1)	Feedforward input to V1 horizontal domain
	(, h_3, u_3)	Feedforward input to V1 vertical domain
	(, h_2, u_2)	Input from lateral conn. in V2 (contour integration)
Feedforward Conn.	(u_1, w_{ff}, u_2)	Feedforward conn. from V1 cell to V2 cel (horizontal)
	(u_3, w_{ff}, u_4)	Feedforward conn. from V1 cell to V2 cell (vertical)
Feedback Conn.	(u_2, w_{fp}, u_1)	Feedback conn. from V2 cell to V1 cell with same orientation preference (V2 horizontal)
	(u_4, w_{fp}, u_3)	Feedback conn. from V2 cell to V1 cell with same orientation preference (V2 vertical)
	(u_2, w_{fo}, u_3)	Feedback conn. from V2 cell to V1 cell with opposite orientation preference (V2 horizontal)
	(u_4, w_{fo}, u_1)	Feedback conn. from V2 cell to V1 cell with opposite orientation preference (V2 vertical)
Lateral Conn.	(u_1,w_{lv1}, u_3)	Lateral inhibition b/t V1 orthogonal domains
	(u_3,w_{lv1}, u_1)	
	(u_2,w_{lv2}, u_4)	Lateral inhibition b/t V2 orthogonal domains
	(u_4,w_{lv2}, u_2)	

This model has the following features. First, activation from V2 cells that are tuned to real and illusory contours send feedback connections to both V1 horizontal and vertical domains. Both feedback connections are excitatory, which is consistent with anatomical studies (Rockland and Douglas 1993, Bullier, et al. 1996). However, the synaptic weights of these two kind of feedback could be different. Second, lateral inhibition between orthogonal domains in V1 and V2 is emphasized. With these two features, the model circuit can give rise to the physiological and psychological findings that V2 feedback to V1 in an illusory contour context is orientation reversal (Ramsden, Chou and Roe 2001) and that real lines interact with illusory contour perception which depends on orientation of the real lines and interacting time (Dillenburger and Roe 2004).

Let's first consider the effect of orientation reversal in V1. There are several possible feedback connection patterns that can lead to the orientation reversal in V1 in an illusory contour context. One mechanism that can lead to orientation reversal might be direct inhibitory feedback

to V1 parallel domains or excitatory feedback projection which target inhibitory interneurons, as proposed by Ramsden et al 2001. Another possibility is that V2 illusory cells send excitatory feedback to V1 orthogonal domains, and the lateral inhibition from V1 orthogonal domains to parallel domains leads to orientation reversal in V1, as proposed by Roe 2003. These feedback patterns works well in obtaining a reversed activation pattern in V1, nevertheless, they are not consistent with the V2 inactivation study which shows that inactivation of V2 cells can significantly reduce the activities of V1 cells to real line stimulus (Bullier, et al. 1996). This implies that V1 cells do receive a net excitatory feedback from V2 cells at least in processing real line stimulus. If real and illusory contours share processing circuit, the two kind of feedback patterns mentioned above are unlikely to give rise to the enhanced activity in V1 cells in a real contour context.

How could V2 feedback to V1 parallel domains exhibits a net excitatory effect in real contour processing and a net inhibitory effect in illusory contour processing? One possibility is that our brain uses two different feedback circuits in processing real and illusory contours. Another possibility is that a common feedback circuitry is used in real and illusory processing, and the net effect of the feedback (excitatory or inhibitory) is self-adaptive to the stimulus context (real or illusory). The model circuit proposed in this section is a self-adaptive system.

Let's start by conceptualize how this is achieved. If this circuit is processing illusory contour information, cell u_2 first gets activated by the contour integration signals that comes laterally (see previous section for detail). This activation feeds back to both u_1 and u_3 with synaptic weights w_{fp} and w_{fo} respectively. After cell u_3 is activated, it inhibits u_1 through lateral inhibition w_{lv1}. Roughly speaking, if the inhibition that follows a $u_2 \rightarrow u_3 \rightarrow u_1$ route outweighs the excitatory feedback $u_2 \rightarrow u_1$, u_1 should receive a net inhibition from u_2.

Now consider the condition when this circuit is processing real contours. Unlike the illusory condition above, in real contour processing, V1 oriented cells receive direct feedforward input from LGN and get activated first. Suppose the real stimulus is oriented at 0 deg, u_1 gets

activated first. This activation is fed forward to V2 neuron u_2 which has the same orientation preference as u_1. Cell u_2 then send excitatory feedback connections to both u_1 and u_3. Note that u_3 already receives lateral inhibition from u_1, so it probably will not fire and thus no inhibition is sent to u_1. In this way, u_1 has a net excitatory feedback from u_2. The excitatory-excitatory loop between u_1 and u_2 is positive feedback and not stable. Inhibition from cell u_3 provides a protection mechanism from the system being too active. If firing rate of u_1 is high enough, the net input to u_3 exceeds the cell's threshold and will thus drive cell u_3, which in turn inhibits cell u_1 and protects u_1 from unstable increasing of firing rate.

Although the above discussion describes the mechanism of the proposed model circuit quite well, it is not sufficient to study the dynamics of the model circuit accurately. To that end, I use the following differential equations to describe the system

$$\tau_r \frac{dv_1}{dt} = -v_1 + F\left(h_1 + w_{fp} v_2 + w_{lv1} v_3 + w_{fo} v_4\right)$$

$$\tau_r \frac{dv_2}{dt} = -v_2 + F\left(h_2 + w_{ff} v_1 + w_{lv2} v_4\right)$$

$$\tau_r \frac{dv_3}{dt} = -v_3 + F\left(h_3 + w_{lv1} v_1 + w_{fo} v_2 + w_{fp} v_4\right)$$

$$\tau_r \frac{dv_4}{dt} = -v_4 + F\left(h_4 + w_{ff} v_3 + w_{lv2} v_2\right)$$

(2.4.1)

In equations 2.4.1, v_1 through v_4 are the firing rates of neurons u_1 through u_4, F is activation function, which is usually a saturation function that is bounded from both above and below. Note that each of the equations follows the firing rate model (equation 2.3.8) introduced in section 2.2.

The model described by equations 2.4.1 is able to account for the orientation reversal pattern in V1 as explained above. However, it is not sufficient if we want to study real-illusory contour interaction in V1 and V2, because the interaction effects were shown to be dependent not only on the orientation of real lines, but the timing of interaction as well. Equations 2.4.1 describes the behavior of the model circuit on the assumption that the presynaptic activation

arrives at postsynaptic neuron in no time. It works well in approximating the time course of firing rate of the postsynaptic neuron with the changing firing rate of a presynaptic neuron, but fails in a situation where timing of the activation are not synchronized. Thus, a modified model should be established to take into account the time delay of transduction of neuronal activation, so that the timing effects of real-illusory contour interaction can be studied.

The modification can be made simply by changing the ordinary differential equations (ODE) 2.4.1 into delay differential equations (DDE) with constant delay,

$$\tau_r \frac{dv_1}{dt} = -v_1 + F\left(h_1(t) + w_{fp}v_2(t-\tau_{fbk}) + w_{lv1}v_3(t-\tau_{lv1}) + w_{fo}v_4(t-\tau_{fbk})\right)$$

$$\tau_r \frac{dv_2}{dt} = -v_2 + F\left(h_2(t) + w_{ff}v_1(t-\tau_{ff}) + w_{lv2}v_4(t-\tau_{lv2})\right)$$

$$\tau_r \frac{dv_3}{dt} = -v_3 + F\left(h_3(t) + w_{lv1}v_1(t-\tau_{lv1}) + w_{fo}v_2(t-\tau_{fbk}) + w_{fp}v_4(t-\tau_{fbk})\right)$$

$$\tau_r \frac{dv_4}{dt} = -v_4 + F\left(h_4(t) + w_{ff}v_3(t-\tau_{ff}) + w_{lv2}v_2(t-\tau_{lv2})\right)$$

(2.4.2)

,where τ_{fbk} is the time delay of activation conduction on a feedback projection; τ_{ff} is the time delay on a feedforward connection; τ_{lv1} and τ_{lv2} are the time delay of lateral inhibition in V1 and V2 respectively. DDE 2.4.2 is the mathematical description of the model circuit I proposed in Figure 11.

DDE 2.4.2 can be viewed as the differential equations to describe a linear system where h1 through h4 are input to the system and v1 through v4 are the system output (Figure 12). Note that h1 through h4 are also the neuronal activations input to the model circuit of V2 feedback to V1 in illusory contour processing, and that v1 through v4 consist of the response of this circuit. Thus, studying the input-output relationship of this system could reveal how real lines interact with illusory contour perception.

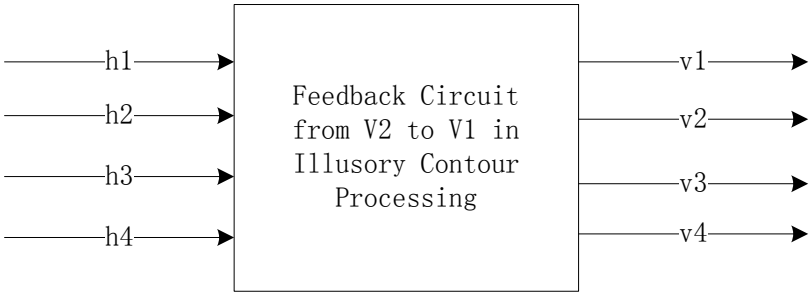

Figure 12. Model circuit as a linear system. Studying the input-output relationship of this system could reveal how real lines interact with illusory contour perception.

CHAPTER III

COMPUTER SIMULATION AND RESULTS

In this chapter, I conduct computer simulation on the model of contour integration in V2 and the model circuit of feedback from V2 to V1 in illusory contour processing. For the model of contour integration in V2, I will show how the spatial weighting function of V2 lateral connections evolves with time and how this kind of process give rise to the receptive field configuration of a V2 bipole cell. To this end, I solve the nonlinear differential equation 2.3.6 numerically using fourth-order Runge-Kutta scheme with adaptive step size control. For the model circuit of feedback from V2 to V1 in illusory contour processing, I conducted several computational experiments to illustrate the different model circuit responses given different input patterns, which simulate the situation of real contour processing, illusory contour processing and interaction of real and illusory contours by solving the delayed differential equations 2.4.2 with second-order Runge-Kutta algorithm. All simulations were conducted with MATLAB 6.5 (Mathworks) software.

Contour Integration in model V2

In Section 2.3, we derived a differential equation 2.3.6 to describe the process of activity-dependent neuronal modification which can lead to the angle distribution of synaptic weights of lateral connections. Let's rewrite this equation here,

$$\tau_w \frac{dw(n,m)}{dt} = (v(n,m) - \varepsilon)u(n,m) \tag{2.3.6}$$

where,

$$v(n,m) = w_{ff} f\left(n\frac{2\pi}{N}\right) + w(n,m)u(n,m)$$

$$\varepsilon = \frac{\sum_{w>0} v(n,m)}{N|_{w>0}}$$

Here, *w(n,m)* is the synaptic weight of lateral connection from a neuron at the angle position of *n* and with a orientation preference of *m*, and *u(n,m)* is the firing rate of this neuron; w_{ff} is the synaptic weight of feedforward connection from V1; *f* is the orientation tuning function of the V1 cell with preferred orientation of zero degree; N is the number of angle positions taken into account (larger N leads to high precision). τ_w is the time constant of synaptic weight change.

In computer simulation, the parameters were chosen as follows: $\tau_w = 1$, $w_{ff} = 1$, N=36. f is chosen as a cosinusoidal function with normalized amplitude,

$$f(\vartheta) = 0.5(cos\ 2\vartheta + 1)$$

thus, when the stimulus is optimally oriented, *f* returns a normalized firing rate of 1. Initial value of differential equation 2.3.6 is $w(n,m)|_{t=0} = 1$, implying synaptic weights exhibits no angle specificity at the initial state.

The result from solving equation 2.3.6 numerically with fourth-order Runge-Kutta algorithm is depicted in Figure 13. The relationship between synaptic weighting function and axis angle θ and orientation preference φ at t=20 was depicted. As clearly shown on the, the synaptic weight peaks at 4 positions: (θ, φ)=(0,0), (0, 180), (180, 0) and (180, 180). This is consistent with our expectation, because the synaptic weight are expected to cluster around horizontal orientation, which is the assumed preferred orientation of the bipole cell (cell p in Figure 9). And this confirms the anatomical finding that lateral connections in cortex contact cells of similar orientation preference tend to be aligned in the cortical map along directions that correspond to the orientational preference (Bosking, et al. 1997).

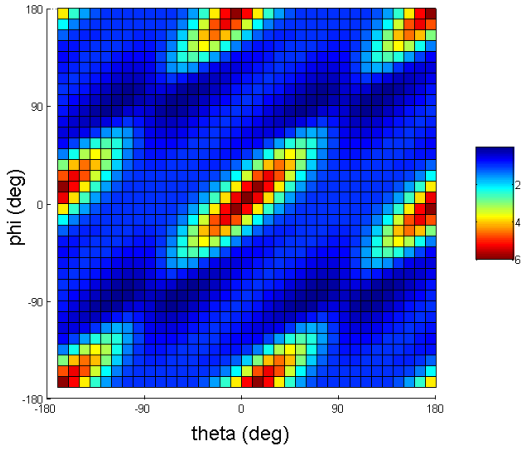

Figure 13 Synaptic weights distribution as a function of axis angle and orientation preference. Theta is the angle position of the distant input cell relative to the horizontal bipole cell located at (0,0) and phi is the orientation preference of the input cell (See Figure 9). Spatial weighting function at t=20 was depicted, when synaptic weights starts to show peaks and valleys. Four peaks were found on the figure considering the periodical characteristic of theta and phi.

The evolution of synaptic weight with time is illustrated in Figure 14. For a certain time t_0, the distance from a point on the surface ($w\cos\theta$, $w\sin\theta$, t_0) to the point $(x,y,t)=(0,0,t_0)$ is the synaptic weight of the horizontal connection when the distant input cell was located at the angle potion of θ. In accord with our expectation in Section 2.3, the computer simulation does show a gradual change from no angle preference of the synaptic weights (circle at the bottom) to a figure-eight shaped synaptic weight distribution. And this figure-eight shaped distribution will be further squashed along x-axis until it becomes something like a straight line along x-axis. The extent of squashing depends on the critical period of visual system development. If the critical period is relatively short, one could expect a relatively fat figure-eight distribution, whereas in a long critical period, this kind of distribution is more elongated along x-axis.

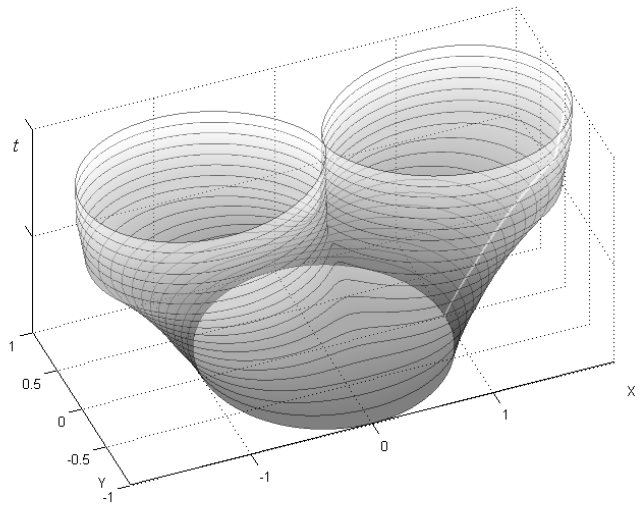

Figure 14. The evolution of synaptic weight distribution with time. Horizontal planes were used to describe synaptic weights as a function of angle position of the distant input cell (θ in Figure 9). For a certain time t_0, the distance from a point on the surface ($w\cos\theta$, $w\sin\theta$, t_0) to the point $(x,y,t)=(0,0,t_0)$ is the synaptic weight of the horizontal connection when the distant input cell was located at the angle potion of θ. A gradual change from no angle specificity of the synaptic weight(circle at the bottom) to a figure-eight shaped synaptic weight distribution is observed.

According to Equation 2.3.1, the spatial weighting function of bipole cell $w(r,\theta,\varphi)$ could be reconstructed by multiplying the factor of angle $w(\theta,\varphi)$ and the factor of distance $w(r)$. We have already solved the spatial weighting function dependent on angle in the above discussion, as shown in Figure 13. Here I use a Gaussian function to model the distance factor $w(r)$. The rebuilt spatial weighting function is demonstrated by Figure 15, in which both horizontal and vertical axis are measured in a unit of degree in visual space. So it can also be viewed as the receptive field of a V2 bipole cell positioned at (0,0) and with a horizontal orientation preference. The Gaussian radius in $w(r)$ was chosen as 7 deg in visual space, so that the resulting receptive field would be elongated horizontally about 20 deg in visual space. In Figure 15, a figure-eight configuration can be easily observed, which goes along with our expectation of a bipole cell receptive field that contains two spatially separate lobes. The spatial weight is maximum along the central horizontal line, and the fanning out part will be able to complete contours with curvature.

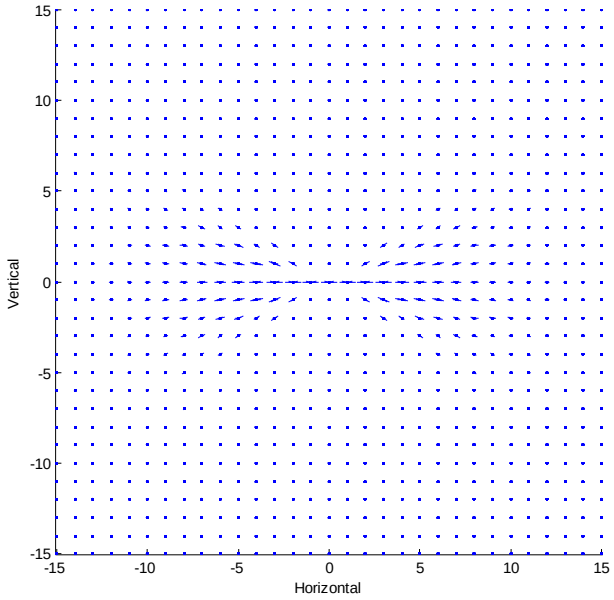

Figure 15. Reconstructed receptive field of V2 bipole cell. Figure was depicted in visual space, and both axis are measured in a unit of degree. A 2D Gaussian function with Gaussian radius =7 deg was used as spatial filter to the weighting function dependent only on angle position and orientation preference (as in Figure 13 and 14). A figure-eight shaped receptive field with two separate lobes can be observed.

The resulting spatial weighting function can be used as a spatial filter in the simulation of contour integration process, which is not included in this paper.

Feedback from V2 to V1 in Illusory Contour Processing

In last chapter, I proposed a model circuit for the feedback from V2 to V1 in illusory contour processing. This circuit utilizes a push-pull mechanism to realize the orientation reversal pattern in illusory contour context and positive feedback in real contour context. A system of delay differential equations 2.4.2 were established in order to describe the model circuit behavior. In this section, a further examination of the circuit behavior will be made by solving equations 2.4.2, and a possible mechanism of real and illusory contour processing in low order visual areas (V1 and V2) will be proposed.

The general method of computer simulation is as follows. Delay differential equations 2.4.2 were solved numerically using MATLAB (Mathworks) function dde23, which is based on second and third order Runge-Kutta algorithm. The system responses were studied in different input patterns, which assemble the situations of real contour processing, illusory contour processing, and real-illusory contour interaction with different orientation, contrast and interacting time.

The parameters in equations 2.4.2 were selected arbitrarily. Delay times on a feedback connetion τ_{fbk} and on a feedforward connetion τ_{ff} were set to 10 msec, which is consistent with physiological findings that feedforward and feedback connections have a similar conduction velocity (Girard et al. 2001) and that V1 activation to illusory contours were lagged about 10 msec than V2 activation to illusory contour stimulus (Lee and Nguyen 2001). Delay times of lateral inhibition between orthogonal domains in V1 and V2 τ_{lv1} and τ_{lv2} were set to 30msec, because lateral connection has a significantly lower conduction velocity than feedforward and feedback connections. The synaptic weights of connections in the model circuit were set as follows, w_{ff}=1, w_{fp}=0.4, w_{fo}=0.6, w_{lv1}=-0.5, w_{lv2}=-0.5.

Activation function F in equations 2.4.2 used in computer simulation is defined as a linear threshold function $F(u) = [u - \gamma]_+$, where γ is threshold and $[\ ]_+$ is half wave rectification. In simulation, $\gamma = 30$. Here, 30 is a measure of relative strength of firing rate, rather than the absolute value of firing rate.

Real and Illusory Contour Representation in V1 and V2

The model circuit behavior was first evaluated in a real line context. When I first proposed the model, I made a conceptual analysis of the responses of the circuit when it receives real line stimulus and pointed out that the model circuit should behave as a physical circuit that V2 sends positive feedback to V1. Here computational simulation further confirmed this point.

In order to simulate the situation of real line input, the input pattern of the model circuit was defined as follows: input to cell u_1 in the model circuit, i.e h_1, was defined as a Heaviside function with a onset time of 130 msec, a duration of 50 msec and an amplitude of 100, while other inputs to the circuit (h_2,h_3,h_4) were left zero. One point that requires mentioning is that the amplitude of the inputs and responses of the model circuit represent only the relative value of firing rate, not necessarily the physical value of firing rates. The response of cell u1 in the model circuit was then prepared to its response when model area V2 was deactivated. Deactivation was achieved by disconnecting the contacts of V1 cells and V2 cells in model circuit. To this end, synaptic weights w_{ff}, w_{fp}, w_{fo} were set to zero.

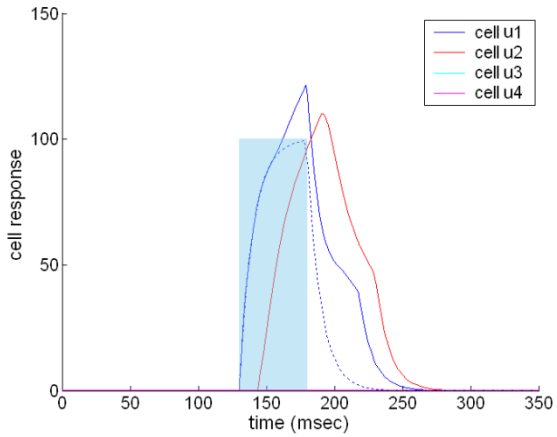

Figure 16. Circuit response to real line stimulation. Blue transparent bar represents the real line input to the circuit (Heaviside function fed into V1 horizontal domain). Blue solid line: cell activity in V1 horizontal domain with V2 feedback; Red solid line: cell activity in V2 horizontal domain; Blue dotted line: cell activity in V1 horizontal domain without V2 feedback.

The result of simulation was depicted in Figure 16. The input to the circuit h_1 corresponding to real line stimulation was represented by the transparent blue bar on the figure. Solid lines are cell responses when V2 feeds back to V1, while dotted lines are cells responses when V2 is deactivated. As can be observed, the V2 cell response to real line (red solid line) is lagged to V1 cell response (blue solid line). V1 cell response when V2 is deactivated is significantly smaller than V2 activated, which is consistent with previous physiological findings (Bullier, et al. 1996).

The model circuit of feedback from V2 to V1 in illusory contour processing should be able to result in orientation reversal pattern in V1 when activated by illusory contour stimuli. Conceptually, we have analyze this point in last chapter. Could computer simulation confirm this? The input pattern of the model circuit to simulate illusory contour stimuli can be defined as zero inputs to V1 cells and non-zero inputs to V2 cells. Suppose the model circuit is processing an illusory contour of 0 degree, cell u_2 will be activated by lateral connections, so I make the input to cell u_2, i.e h_2, a Heaviside function with onset time at 125 msec, a duration of 50 msec and an amplitude of 70. The reason why I make the onset time of h2 125 msec is that the first activation of V2 cell response to illusory contour is at about 125 msec. And amplitude 70 is because cell response to illusory contour is usually less than the response to real contour. The input configuration is illustrated in Figure 17.

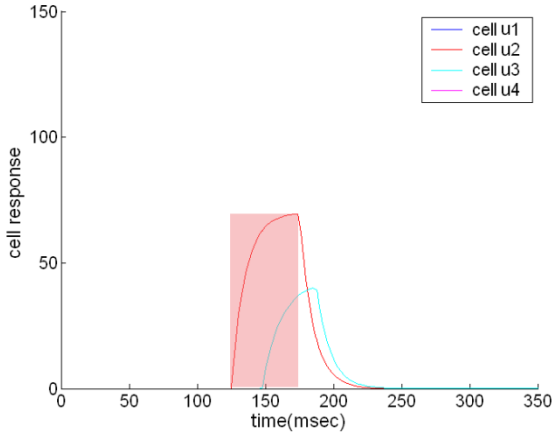

Figure 17. Circuit response to illusory contour stimulation. Red transparent bar represents the illusory line input to the circuit (Heaviside function fed into V2 horizontal domain). Red solid line: cell activity in V2 horizontal domain; Cyan solid line: cell activity in V1 vertical domain. No other activation in this case.

Figure 17 shows the result of simulation. Input was represented by the transparent red bar. Red solid line is the time course of cell u_2 (V2 cell tuned to 0 deg) response to illusory contour stimuli and cyan solid line is the time course of cell u_3 (V1 cell tuned to 90 deg). Figure 17 clearly shows that V1 cell response to illusory contour is significantly delayed compared to V2 cell. And the V1 cell with orientation preference orthogonal to the illusory contour gets activated

while cells tuned to the orientation of illusory contour is not activated. The simulation result is consistent with previous physiological findings (Lee & Nguyen 2001, Ramsden et al. 2001).

Hypothesized Brain Mechanism of Contour Perception

The different neural activation pattern in early visual cortex in real and illusory context, as discussed above, might suggest a mechanism how our brain differentiate real lines and illusory contour. I hypothesize that contour perception depends on the comparison between orthogonal domains in both V1 and V2. First, the type of contour perceived relies on the sign of comparison in V1 and V2. If the activation pattern are equal in V1 and V2, a real line perception will be produced, otherwise, an illusory contour perception forms. Second, the perceptual strength of contours might depend on the value of difference between orthogonal domains in V1 or V2: larger difference leads to stronger perceptual strength, both real and illusory. For example, in the real line simulation above (see Figure 16), both cells with an orientation preference of 0 deg in V1 and V2 were activated stronger than cells with 90 deg orientation preference. According to our hypothesis, this kind of activation pattern should result in a real line perception. On the other hand, if cells in V2 with 0 deg orientation preference fire stronger than those with 90 deg preference, while in V1 a reversed pattern was found, as in the case of Figure 17, an illusory contour should be perceived according to our hypothesis. If the firing rate difference between horizontal and vertical domains in V1(or V2) is not significant, the contour perception will be weakened, otherwise the perception will be enhanced. This idea is summarized in Figure 18.

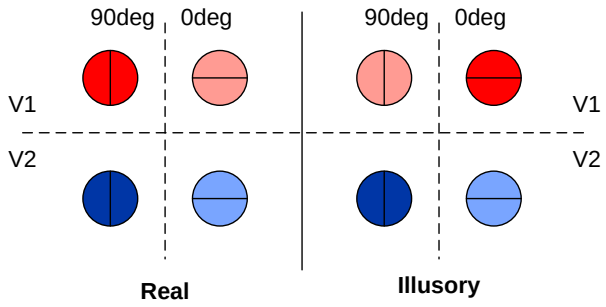

Figure 18 Hypothesized brain criteria of contour perception. Contour perception might rely on the comparisons between orthogonal domains in both V1 and V2. Type of contour perceived relies on the sign of comparison in V1 and V2. The accordance of comparison signs in V1 and V2 give rise to real line percept and different comparison signs in V1 and V2 lead to illusory contour percept. The perceptual strength of contours depends on the difference value of firing rates between orthogonal domains: larger difference leads to stronger perceptual strength, both real and illusory.

Real-Illusory Interaction

The model circuit of feedback from V2 to V1 in illusory contour processing was then tested for the interaction effects between real lines and illusory contours. Resent psychophysical study (Dillenburger and Roe 2004) has suggested a real-interaction effect dependent on orientation, real line contrast and interaction time. The most consistent effects found are orthogonal low contrast summation effects at an early interaction time (50 msec), parallel low contrast interference at later time (125 msec) on, and a reversal of orthogonal line effects over all contrast ranges from summation to interference at times of 125 msec to 150 msec. Our simulation results confirmed these psychophysical findings.

Exp.1 Early Interaction of Parallel Real Line. Figure 19 is the simulation result of the early interaction effect of parallel real line and illusory contour. Real and illusory inputs to the circuit are depicted by blue and red transparent bars on the figure respectively. An early real line stimulus starting at 50 msec was simulated by a Heaviside function with onset time=50msec, duration=25msec and amplitude=50. Illusory contour input to the circuit was given by the

Heaviside function with onset time= 125msec, duration=50msec and amplitude=70. As can be observed from Figure 19, the time course of cell activities after illusory input was only changed slightly (if not) when the early real parallel line stimulus was given. Thus I will conclude that the perception of illusory contour is not affected by an early presentation of parallel real lines, which is consistent with psychophysical evidence that no significant effect of parallel real lines was discovered on the perception of illusory contour.

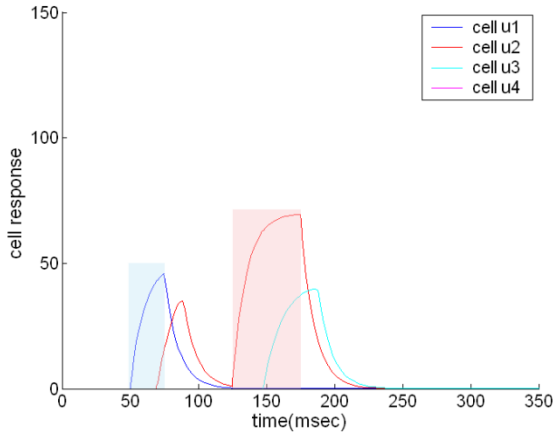

Figure 19. Circuit response of early interaction of parallel real line. Blue and red transparent bars represent the real and illusory horizontal line inputs respectively. Blue solid line: cell activity in V1 horizontal domain; Red solid line: cell activity in V2 horizontal domain; Cyan solid line: cell activity in V1 vertical domain.

Exp.2 Early Interaction of Orthogonal Real Line. A similar computational experiment was conducted to study the interaction of early presented orthogonal real line and illusory contour. Fig 20 is the simulation result, on which inputs to the model circuit is indicated by transparent bars. The input pattern to model circuit is identical to exp.1 expect that the real line input was to the V1 vertical domain with a duration of 50 msec. Similar to Exp 1, the simulation result in Fig 20 also suggested a slightly changed time course of illusory contour representation in V1 and V2 with the presence of early orthogonal real lines. According to the hypothesized brain criteria of contour perception we proposed in last section, the perception of illusory contour should not be affected by orthogonal real line. This is inconsistent with the psychophysical finding that early presence of orthogonal real lines will have a summation effect on the perception of illusory

contour. How could this be explained? Dillenburger et. al suggested in their model that this summation effect was because illusory contour induction phase has not ended at an early time of 50msec, orthogonal real line abutting to the illusory contour might activate end-stopped cells in V1, which add information to the induction of illusory contour, thus leading to a stronger illusory contour perception. In our model circuit, the induction of illusory contour was not included, and that's the reason why it can not explain this summation effect.

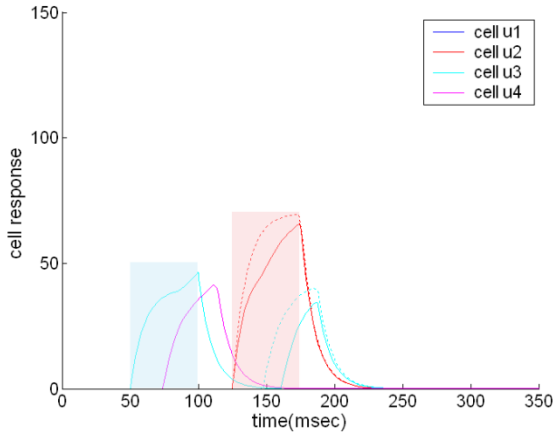

Figure 20. Circuit response of early interaction of orthogonal real line. Blue and red transparent bars represent the real (vertical) and illusory (horizontal) line inputs respectively. Red solid line: cell activity in V2 horizontal domain with interaction; Cyan solid line: cell activity in V1 vertical domain with interaction; Red dotted line: cell activity in V2 horizontal domain without interaction; Cyan dotted line: cell activity in V1 vertical domain without interaction.

Exp 3. Later Interaction of Parallel Real Line. Later interaction effect of parallel real lines on the perception of illusory contour can be simulated by shifting the real line input to 130 msec. The response of the model circuit was first tested with a suprathreshold parallel real line. A Heaviside function input to horizontal domain in V1 with a onset time of 130msec, duration of 50msec and amplitude of 50 was used to simulate the suprathreshold real line input. Illusory contour input was identical to that of Exp 1 and 2. The circuit response was depicted on Figure 21. Dotted lines are the time course of cell responses when no real line stimulus was presented whereas solid lines are the time course with real line stimulus. As can be observed on Fig 3a, the suprathreshold parallel real line stimulus will enhance the cell response in V1 horizontal domain (blue line) and V2 horizontal domain (red line), while leaving the cell response in V1 vertical

domain (cyan) only slightly changed. The enhancement of firing rate in V1 horizontal domain resulted in a stronger activation in V1 horizontal domain than vertical domain, which is a reversed pattern compared to the pattern when only illusory stimulus was presented. According to the hypothesis I made in last section, the accordance of activation pattern in V1 and V2 should lead to a real parallel (horizontal) line perception, and the perception of illusory contour should be eliminated.

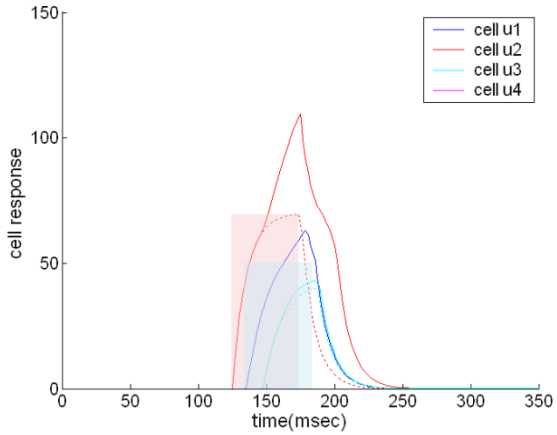

Figure 21. Circuit response of later interaction of suprathreshold parallel real line. Blue and red transparent bars represent the real and illusory horizontal line inputs respectively. Blue solid line: cell activity in V1 horizontal domain; Red solid line: cell activity in V2 horizontal; Cyan solid line: cell activity in V1 vertical domain; Red dotted line: cell activity in V2 horizontal domain without interaction; Cyan dotted line: cell activity in V1 vertical domain without interaction.

What if the parallel real line was perceptually subthreshold? I used a Heaviside function starting at 130msec, duration of 50msec and amplitude of 20 as real parallel line input. Figure 22 shows the simulation result. Compared to suprathreshold real line case in Figure 21, the extent of cell response enhancement in V1 and V2 horizontal domains were smaller, and the activation pattern in V1 was not reversed (V1 vertical domains were still activated stronger than V1 horizontal domains). In this case, illusory contour should still be perceived, but the perceptual strength should decrease due to the decrease of activity difference between V1 horizontal and vertical domains. The simulation result is consistent with psychophysical evidence.

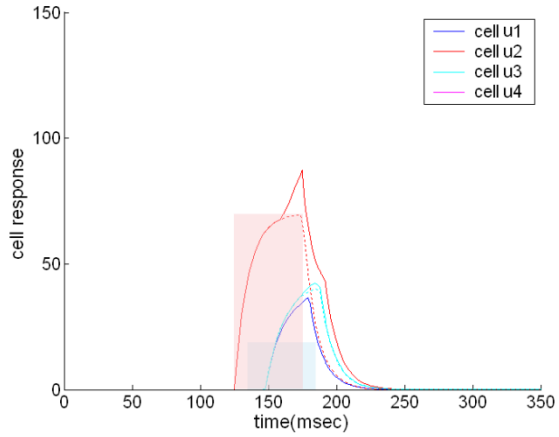

Figure 22. Circuit response of later interaction of subthreshold parallel real line. Blue and red transparent bars represent the real and illusory horizontal line inputs respectively. Blue solid line: cell activity in V1 horizontal domain; Red solid line: cell activity in V2 horizontal; Cyan solid line: cell activity in V1 vertical domain; Red dotted line: cell activity in V2 horizontal domain without interaction; Cyan dotted line: cell activity in V1 vertical domain without interaction.

Exp 4. Later Interaction of Orthogonal Real Line. The last computational experiment conducted was to evaluate the interaction between orthogonal real line and illusory contour at a later interaction time (from 125msec on). The inputs to the circuit are identical to that in Exp 3 except that the real stimulus input was fed into V1 vertical domain. The circuit response was tested in both subthreshold real line condition (Figure 23) and suprathreshold real line condition (Fig 24). In the subthreshold condition, an increased firing rate in V1 vertical domain can be observed while V2 horizontal domain exhibited little change of cell activity (See Figure 23). According to the hypothesis we made earlier, an enhanced perception of illusory contour arise.

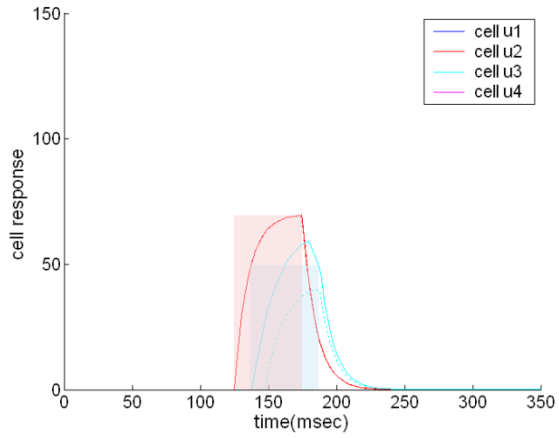

Figure 23. Circuit response of later interaction of subthreshold orthogonal real line. Blue and red transparent bars represent the real (vertical) and illusory (horizontal) line inputs respectively. Red solid line: cell activity in V2 horizontal domain; Cyan solid line: cell activity in V1 vertical domain; Red dotted line: cell activity in V2 horizontal domain without interaction; Cyan dotted line: cell activity in V1 vertical domain without interaction.

In suprathreshold condition, the orthogonal real line stimulus not only elicit an increase in the activity of V1 vertical domain, but the activity of V2 vertical domain as well (Figure 24). V2 horizontal domain hardly changed its response in the presence of orthogonal real line, and was still activated more strongly than the activity of V2 vertical domain. Applying the hypothesized criteria of contour perception again, illusory contour should still be perceived, but due to the decrease of activity contrast between V2 horizontal and vertical domains, the perception strength should decrease. Moreover, as we can expect, if the orthogonal real line stimulus was even stronger, the activation in V2 vertical domain will outweigh the activation in V2 horizontal domain, in which case a real orthogonal (vertical) line will be perceived. In psychophysical study, an change from summation effect to interference indeed occurred when an abutting orthogonal real line interacted with the illusory contour at 125-150msec.

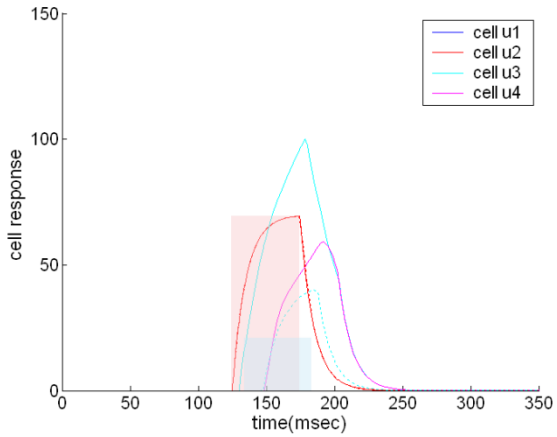

Figure 24. Circuit response of later interaction of suprathreshold orthogonal real line. Blue and red transparent bars represent the real (vertical) and illusory (horizontal) line inputs respectively. Red solid line: cell activity in V2 horizontal domain; Cyan solid line: cell activity in V1 vertical domain; Purple solid line: cell activation in V2 vertical domain; Red dotted line: cell activity in V2 horizontal domain without interaction; Cyan dotted line: cell activity in V1 vertical domain without interaction.

CHAPTER IV

SUMMARY AND DISCUSSION

In this paper, I proposed a computational model for illusory contour processing in early visual areas. In the model, illusory contour perception is a process which contains multiple stages at different brain areas. The first stage of processing is image feature measurement in model V1, where local contrast orientation is measured by cells of oriented receptive fields and local line ends are measured by hypercomplex end-stopping cells. Then the resulting activities in V1 are fed into V2 cells with non-classical bipole property (Grossberg et al. 1997, Neumann and Sepp 1999, Domijan et al. 2007), which integrate the activities from two further apart locations and fire at a position that falls in between. The integrated illusory contour information resides in model V2 was then delivered to model V1 through feedback connection. The feedback was able to give rise to orientation reversal pattern (Ramsden, Chou and Roe 2001) in V1 in the context of illusory contour.

The stage of contour integration by V2 cells with bipole property and feedback from V2 to V1 was discussed in detail in the paper. First, I proposed a model based on activity-dependent synaptic modification to explain the mechanism of lateral connection formation. With the assumption that straight lines are the major visual experience leading to the specific configuration of bipole cell receptive field, a system of non-linear differential equations that depends on internal states of equation solution was built to describe the model. This system of differential equations was solved numerically within a fourth-order Runge-Kutta scheme. The resulting distribution of spatial weighting function across axis angle and orientation preferences goes along with conceptual analysis and the reconstructed receptive field of a “contour integration” bipole cell in V2 is consistent with the anatomical finding that long range lateral connection in early

visual cortex setup between cells with similar orientation preferences and that the axis orientation of the lateral connection tend to be the same direction of the preferred orientation of cells.

Second, I proposed a model circuit for the feedback from V2 to V1 in illusory contour processing. This circuit can give rise to orientation reversal pattern in illusory contour context by using a push-pull mechanism between orthogonal orientation domains in model V1. In real line context, this circuit will lead to a net positive feedback effect to parallel V1 domains, which is consistent with the study which suggested inactivation of V2 decreased V1 cell responses (Bullier, et al. 1996). So the simple mechanism of push-pull competition in V1 orthogonal domains well explained the context dependent feedback from V2 to V1 in processing real (positive feedback) and illusory contours (negative feedback). To explain the psychophysical finding that real line can interact with illusory contour perception which is dependent on real line orientation, contrast and interacting time (Dillenburger and Roe 2004), the time lags in activation conduction were introduced to the model circuit of V2 feedback, and a system of delay differential equations based on firing rate model were built to describe the model circuit. The delay differential equations were solved numerically using MATLAB (Mathworks) function dde23, which is based on second and third order Runge-Kutta algorithm, and the circuit behavior in real line condition and illusory contour was confirmed by the differential equation solution. By managing different input patterns to the model circuit, the circuit responses in real-illusory interaction were simulated. Simulation were conducted on the conditions of early interaction (SOA 50msec) of real parallel line and orthogonal line, later interaction (SOA 125msec) of real parallel line and orthogonal line with high and low contrasts. The simulation results were consistent with psychophysical findings.

Third, a brain mechanism for contour perception was proposed. The type of contour perceived was hypothesized to be dependent on the comparison of activation in orthogonal domains in V1 and V2. If the comparison of cell activities in horizontal and vertical domains in V1 and in V2 are reversed in sign, a perception of illusory contour should arise. On the other hand, if the comparison of orthogonal domains are equal in sign in V1 and V2, real line should be

perceived. Further more, the perceptual strength of contour was hypothesized to be dependent on the activation contrast value between orthogonal domains both in V1 and V2. Specifically, if the activation difference between horizontal and vertical domains increases in V1 or V2, the perception of contour (real or illusory) should be enhanced, otherwise, perception strength will be decreased. In model simulation, this hypothesis was used as the criteria for the perceptual outcome of real-illusory interactions.

Although the proposed model framework for the illusory contour processing in early visual cortex is consistent with a number of physiological and psychophysical findings, it leaves several issues to be discussed. One issue is whether early visual cortex is sufficient to elicit an illusory contour percept or whether illusory contour perception is bottom-up, which depends on low level processing, or top-down, which involves cognitive. Traditionally, illusory contour processing has been explained within the cognitive framework (Gregory 1972, Rock and Anson 1979). Illusory contour completion is seen as the attempt to find the most likely solution to a perceptual problem. This view has changed in the past years. Evidence has been found that flavors illusory contour processing in low-level brain areas. In their ground-breaking experiments, von der Heydt et al. 1984 found that a moving illusory bar could elicit V2 neurons in monkeys even when there was nothing inside the receptive field of the neurons. Lee and Nguyen 2001 studies the temporal evolution of neuronal activities in V1 and V2 in response to the static display of Kanizsa figures. They found that the response to illusory contours in V1 in monkeys emerged at about 100ms, significantly later than the emergence of illusory contour response in V2. Other single unit and optical imaging studies also showed representation of illusory contour in V1 and V2 (Grosof et al. 1993, Sheth et al. 1996, Ramsden et al. 2001).

However, recent human fMRI studies (Mendola et al. 1999) found Kanizsa figures elicited significant responses in the lateral occipital region (LOC), but only weak response in the human early visual areas. Murray et al. 2002 replicated the results by Mendola et al. and measured latencies to illusory figure response onset with EEG and fMRI. They found that the earliest VEP

modulation to illusory contour stimuli over LOC scalp, which implies a high order modulation of illusory contour perception. In a lesion study, Huxlin et al. 2000 observed on the impairment of a monkey's ability to see illusory contours as a result of lesion in the inferotemporal cortex (IT). These findings ignite the debate of whether illusory contour perception is an early or late process. Montaser-Kouhsari et al. 2007 used an fMRI adaptation paradigm to entangle this question. In a series of elegant experiments, they showed that fMRI adaptation detected orientation-selective responses to illusory contour exist in almost all visual areas.

If illusory contour perception receives the modulation from high visual areas, what might be the possible model of illusory contour processing? Lee 2002 proposed a possible scenario that information inducing illusory contour propagates to high visual area rapidly through direct feedforward computation, which generates rough hypotheses about the shape and figures in the scene. These hypotheses then propagate down the visual hierarchy to guide the early visual areas to work out the details, constructing a precise representation of illusory contour using the intrinsic circuitry in V1 and V2. As the illusory contour becomes clear and precise in the early visual areas, the global shape percept of the illusory figure starts to emerge in higher visual areas (Lee 2002). From this perspective, the computation of illusory contour involves both early and late processes.

The model proposed in this paper does not contradict with the high level areas involvement in illusory contour processing. Although focused mainly on the illusory contour processing in lower-tier visual areas, my model doesn't exclude the possibility of high order modulation in illusory contour inducing process. In fact, signals from high-order areas such as lateral occipital complex (LOC) could serve as a gating signal for the contour completion process in model V2. It is possible that long-range horizontal connections in V2 are not able to give rise to a robust representation of the illusory contour "filled in", and with the guidance of neural signal from high areas which carries an estimation of the illusory contour, the neural activities in V2 that fit the estimation will be enhanced and those do not fit will be depressed.

In sum, the proposed model framework for the illusory contour processing in early visual cortex in this thesis is consistent with a number of physiological and psychophysical findings and might be able to explain the mechanism of illusory contour perception in V1 and V2. However, due to the lack of physiological and anatomical data concerning the interaction between early visual cortex and areas higher in visual hierarchy, the contribution of higher order areas to the perception of illusory contour was not studied by this computational work. Additional empirical investigations are needed before we can address the question of how we can see things beyond reality.

APPENDIX

A. MATLAB Code for simulation of the bipole receptive field

```
%--------------------------
% File: Equ236_Sol.m
% Desc: Solving Equ 2.3.6
%--------------------------

w0=ones(36*36,1); %initial value
[t,w]=ode45(@hebb,[0 20],w0); %solve equ 2.3.6 using ode45
%convert to 3D matrix weight(n,m,weight_val)
for i=1:36
    for j=1:36
        weight(i,j,:)=w(:,36*(i-1)+j);
    end
end
save weight_sim t w weight;

%--------------------------
% equation 2.3.6
function dw=hebb(t,w)
N=36;wff=1;eps=0;v=0;c=0;s=0;
dw=zeros(N*N,1);
% put synaptic weight at position (n,m) to zero
% if less than 0, calculate the sum of non-zero
% weights to get the sliding threshold epsilon
for i=1:N          % n, the index representing theta
    for j=1:N      % m, the index representing phi
        ind=(i-1)*N+j;
        if (w(ind)>0)    % equation 2.3.7
           c=c+1;
           v=wff*(cos(2*i*2*pi/N)+1)/2+w(ind)*wff*...
                  (cos(2*(i-j)*2*pi/N)+1)/2;
           s=s+v;
        else
           w(ind)=0;
        end
    end
end
eps=s/c; % epsilon equals the average value of
         % existing non-zero synaptic weights
for n=1:N
    for m=1:N
        ind=(n-1)*N+m;
      if (w(ind)>0)
          u=wff*(cos(2*(n-m)*2*pi/N)+1)/2;
          dw(ind)=(wff*(cos(2*n*2*pi/N)+1)/2+w(ind)*u-eps)*u;
      else
          dw(ind)=0;
      end
    end
end
```

```
%--------------------------
% File: DrawFig13.m
% Desc: Draw figure 13
%--------------------------
%load data
clear;
load weight_sim;
theta=zeros(36,36);
phi=zeros(36,36);
a=[-170:10:180];
for k=1:36
    theta(k,:)=a;
end
phi=theta';
surf(theta,phi,weight(:,:,20));
axis([-170 180 -170 180]);
axis equal;


%--------------------------
% File: DrawFig14.m
% Desc: Draw figure 14
%--------------------------
%Fig 14 in the thesis used a higher resolution
i=1:1:36;
theta=2*pi/36*i;
w0=zeros(36,4000);
%pick up the weighting values where theta==phi
for k=1:36
    w0(k,:)=weight(k,k,:);
end
x=cos(theta(:));
y=sin(theta(:));
for j=1:1:20
    wl=w0(:,j);
    X(:,j)=wl.*x;
    Y(:,j)=wl.*y;
    Z(:,j)=j*ones(36,1);
end
save weight_sim w1;
surf (X,Y,Z);


%--------------------------
% File: DrawFig15.m
% Desc: Draw figure 15
%--------------------------
% load data
load weight_sim;
% use a vector map to simulate the bipole RF
[x,y]=meshgrid(-15:1:15,-15:1:15);
r=sqrt(x.^2+y.^2); % distance from distant input cell to bipole cell
% 2D Gaussian function as distance factor w(r)
gaussflt=25*normpdf(r,0,7);
% theta value on the grid points
the=atan(y./x)/(2*pi)*360;
the(16,16)=0; % exclude (0,0) point to prevent "devided by zero error"
```

```
the_index=round(the/10)+18; % index of theta in the weighting matrix
figure,hold on;
% vector map display
for phi_index=1:36
    mod=[];
    angle=phi_index*10*2*pi/360-pi;
    for i=1:31
        % mod is the synaptic weight value
        mod=[mod weight(the_index(:,i),phi_index,3000)];
    end
    % filtered by Gaussian function w(r),
    % 1/600 as a adjustment coefficient
    % for suitable screen display
    mod=mod/600.*gaussflt;
    px=cos(angle)*mod;
    py=sin(angle)*mod;
    % draw vector map
    quiver(x,y,px,py,0,'.');
    axis image;
end
hold off
```

B. MATLAB code for simulation of V2 feedback model

```
%--------------------------------
% File: V1V2Interaction.m
% Desc: Simulation of
%       Real-illusory interaction
%       with V2 feedback model
%--------------------------------
% Set parameters here
p.wf=1;
p.wbp=.4;
p.wbo=.6;
p.wlv1=-.5;
p.wlv2=-.5;
% Change inputs to the model circuit
p.h1=0;
p.h2=70;
p.h3=0;
p.h4=0;

% solving delay-differential equation 2.4.2
sol = dde23(@ddefun,[10 30],[0; 0; 0; 0],[0, 1000],[],p);
% plot cell responses (u1~u4)
hold on;
plot(sol.x,sol.y(1,:),'b:','LineWidth',1);
plot(sol.x,sol.y(2,:),'r:','LineWidth',1);
plot(sol.x,sol.y(3,:),'c:','LineWidth',1);
plot(sol.x,sol.y(4,:),'m:','LineWidth',1);
hold off;
axis([0 350 0 150]);

%---------------------------
% equation 2.4.2
function dv=ddefun(t,v,Z,p)
ylag1=Z(:,1);
ylag2=Z(:,2);
dv=zeros(4,1);
dv(1)=-v(1)+saturation(p.h1*stepf((t-130)/50)   ...
    +p.wbp*ylag1(2)+p.wlv1*ylag2(3)+p.wbo*ylag1(4));
dv(2)=-v(2)+saturation(p.h2*stepf((t-125)/50)  ...
    +p.wf*ylag1(1)+p.wlv2*ylag2(4));
dv(3)=-v(3)+saturation(p.h3*stepf((t-130)/50)   ...
    +p.wlv1*ylag2(1)+p.wbo*ylag1(2)+p.wbp*ylag1(4));
dv(4)=-v(4)+saturation(p.h4*stepf(t/100)   ...
    +p.wf*ylag1(3)+p.wlv2*ylag2(2));
dv=dv./10; % use a time variable of 10

%---------------------------
%Heaviside function
function y = stepf(x)

if ( x<=1 & x>=0 )
    y=1;
else
    y=0;
end
```

REFERENCES

Amirikian, B. (1999) Chapter 25 In *Modern techniques in neuroscience research*, by U Windhorst and H Jonansson, 689-704. Springer, 1999.

Bosking, W.H., Zhang, Y., Schofield, B., and Fitzpatrick, D. (1997) Orientation Selectivity and the Arrangement of Horizontal Connections in Tree Shrew Striate Cortex. *J. Neurosci.*, **17(6)**, 2112-27.

Bullier, J., Hupe, J.M., James, A., and Girard, P. (1996) Functional interactions between areas V1 and V2 in the monkey. *J Physiol Paris.*, **90(3-4)**, 217-20.

Cunningham, D.W., Shipley, T.F, and Kellman, P.J.(1998) The dynamic specification of surfaces and bounderies. *Perception*, **27(4)**, 403-15.

Dayan, P., and Abbott, L.F.(2001) Chapter 7 In *Theoretical Neuroscience*. The MIT Press, 2001.

Dillenburger, B., and Roe, A.W.(2004) Psychophysical evidence for competition between real and illusory contour processing. *J. Vision*, **4(8)**, 734.

Domijan, D., Setic, M., and Svegar, D.(2007). A model of the illusory contour formation based on dendritic computation. *Neurocomputing*, **70**, 1977-82.

Girard, P., Hupe, J.M., and Bullier, J.(2001). Feedforward and feedback connections between areas V1 and V2 of the monkey have similar rapid conduction velocities. *J.Neurophysiol.*, **85(3)**, 1328-31.

Gregory, R.L.(1972) Cognitive contours. *Nature*, **238**, 51-52.

Grosof, D.H., Shapley, R.M., and Hawken, M.J.(1993). Macaque V1 neurons can signal "illusory contours. *Nature*, **365**, 550-2.

Grossberg, S., and Mingolla, E. (1985) Neural dynamics of perceptual grouping: textures, boundaries, and emergent segmentations. *Percept Psychophys*, **38**, 141-71.

Grossberg, S., Mingolla, E., and Ross, W.D. (1997) Visual brain and visual perception: How does the cortex do perceptual grouping? *Trends Neurosci.*, **20**, 106-11.

Hubel, D.H., and Wiesel, T.N.(1968) Receptive fields and functional architecture of monkey striate cortex. *J. Physiol.*, **195**, 215-43.

Huxlin, K.R., Saunders, R.C., Marchionini, D., Pham, H, and Merigan, W.H.(2000) Perceptual deficits after lesions of inferotemporal cortex in macaques. *Cereb. Cortex*, **10(7)**, 671-83.

Julesz, B. (1960) Binocular depth perception of computer generated patterns. *Bell Syst. Tech. Journal*, **39**, 1125-62.

Kanizsa, G.(1976) Subjective contours. *Sci. Am.*, **234(4)**, 48-52.

Lee, T.S. (2002) The nature of illusory contour computation. *Neuron*, **33(5)**, 667-8.

Lee, T.S., and Nguyen, M. (2001) Dynamics of subjective contour formation in the early visual cortex. *Proc. Natl. Acad. Sci. USA*, **98**, 1907-11.

Mclaughlin, D., Shapley, R., Shelley, M., and Wielaard, D.J. (2000) A neuronal network model of macaque primary visual cortex (V1): Orientation selectivity and dynamics in the input layer 4C. *Natl. Acad. Sci.*, **97(14)**, 8087-92.

Mendola, J.D., Dale, A.M., Fischi, B., Liu, A.K., and Tootell,R. (1999) The representation of illusory and real contours in human cortical visual areas revealed by functional magnetic resonance imaging. *J. Neurosci.*, **19(19)**, 8560-72.

Murray, M.M., Wylie, G.R., Higgings, B.A, Javitt, D.C., Schroeder, C.E., and Foxe, J.J. (2002) The spatiotemporal dynamics of illusory contour processing: combined high-density electrical mapping, source analysis, and functional magnetic resonance imaging. *J. Neurosci.*, **22(12)**, 5055-73.

Neumann, H., and Sepp, W. (1999) Recurrent V1-V2 interaction in early visual boundary processing. *Biol. Cybern*, **81**, 425-44.

Nieder, A. (2002) Seeing more than meets the eye: processing of illusory contours in animals. *J. Comp. Physiol. A*, **188**, 249-60.

Peterhans, E., and von der Heydt, R. (1989) Mechanisms of contour perception in monkey visual cortex. II. contours bridging gaps. *J. Neurosci.*, **9**, 1749-63.

Ramachandran, V.S. (1987) Visual perception of surfaces: a biological theory. In *The perception of illusory contours*, by Petry, S. and Meyer, G.E., 93-108. Berlin Heidelberg New York: Springer, 1987.

Ramsden, B.M., Chou, P.H., and Roe, A.W. (2001) Real and illusory contour processing in area V1 of the primate: a cortical balancing act. *Cereb. Cortex*, **11(7)**, 648-65.

Rivest, J., and Cavanagh, P.(1996) Localizing contours defined by more than one attribute. *Vision Res.*, **36**, 53-66.

Rock, I., and Anson, R. (1979) Illusory contours as the solution to a problem. *Perception*, **8**, 665-81.

Rockland, K.S., and Douglas, K.L. (1993) Excitatory contacts of feedback connections in layer 1 of area V1: an EM-biocytin study in the macaque. *Soc Neurosci.* **19**, 424.

Roe, A.W.(2003) Chapter 5 In *The primate visual system*, 109-38. CRC Press LLC, 2003.

Ross, W.D., Grossberg, S., and Mingolla, E. (2000) Visual cortical mechanisms of perceptual grouping: interacting layers. *Neural Networks*, **13**, 571-88.

Sheth, B.R., Sharma, J., Rao, S.C., and Sur, M. (1996) Orientation maps of subjective contours in visual cortex. *Science*, **274**, 2110-5.

Shmuel, A., et al. (2005) Retinotopic axis specificty and selective clustering of feedback projections from V2 to V1 in the owl monkey. *J. Neurosci.*, **25(8)**, 2117-31.

von der Heydt, R., and Peterhans, E. (1989) Mechanism of contour perception in monkey visual cortex.I. Lines of pattern discontinuity. *J. Neurosci,* **9**, 1731-48.

von der Heydt, R., Peterhans, E., and Baumgartner, G.(1984) Illusory contours and cortical neuron responses. *Science*, **224**, 1260-2.